





Neurons of the inferior olive respond to broad classes of sensory input while subject to homeostatic control

Chiheng Ju^{1,*}, Laurens W.J. Bosman^{1,*} , Tycho M. Hoogland^{1,2,*} , Arthiha Velauthapillai¹, Pavithra Murugesan¹, Pascal Warnaar¹, Romano M. van Genderen¹, Mario Negrello¹  and Chris I. De Zeeuw^{1,2} 

¹Department of Neuroscience, Erasmus MC, 3015 GD Rotterdam, The Netherlands

²Netherlands Institute for Neuroscience, Royal Netherlands Academy of Arts and Sciences, 1105 BE, Amsterdam, The Netherlands

Edited by: Ole Paulsen & Michisuke Yuzaki

Key points

- Purkinje cells in the cerebellum integrate input from sensory organs with that from premotor centres.
- Purkinje cells use a variety of sensory inputs relaying information from the environment to modify motor control.
- Here we investigated to what extent the climbing fibre inputs to Purkinje cells signal mono- or multi-sensory information, and to what extent this signalling is subject to recent history of activity.
- We show that individual climbing fibres convey multiple types of sensory information, together providing a rich mosaic projection pattern of sensory signals across the cerebellar cortex.
- Moreover, firing probability of climbing fibres following sensory stimulation depends strongly on the recent history of activity, showing a tendency to homeostatic dampening.

Abstract Cerebellar Purkinje cells integrate sensory information with motor efference copies to adapt movements to behavioural and environmental requirements. They produce complex spikes that are triggered by the activity of climbing fibres originating in neurons of the inferior olive. These complex spikes can shape the onset, amplitude and direction of movements and the adaptation of such movements to sensory feedback. Clusters of nearby inferior olive neurons project to parasagittally aligned stripes of Purkinje cells, referred to as ‘microzones’. It is currently

Chiheng (Bryen) Ju worked as clinical neurologist for 8 years before starting as a PhD student, first in Neurology at Shanghai Jiaotong University and later in Neuroscience at Erasmus MC in Rotterdam, the Netherlands. After obtaining his PhD he became a post-doctoral fellow with David Kleinfeld at UCSD. **Laurens Bosman** received his PhD in Neuroscience at the Vrije Universiteit Amsterdam, after which he joined Arthur Konnerth’s lab in Munich, Germany. Currently he studies how the cerebellum, as part of a brain-wide network, controls the adaptation of movements in response to sensory feedback in health and disease. **Tycho Hoogland** is an assistant professor at the Department of Neuroscience at Erasmus MC working to understand how the olivo-cerebellar circuit contributes to sensorimotor integration using a combination of *in vitro*, *in vivo* and behavioural approaches. He also leads the development of miniaturized microscopes at the Netherlands Institute for Neuroscience.



*These authors contributed equally.

This article was first published as a preprint. Ju C, Bosman LWJ, Hoogland TM, Velauthapillai A, Murugesan P, Warnaar P, Negrello M & De Zeeuw CI. (2018). Neurons of the inferior olive respond to broad classes of sensory input while subject to homeostatic control. *bioRxiv*. <https://doi.org/10.1101/379149>.

unclear to what extent individual Purkinje cells within a single microzone integrate climbing fibre inputs from multiple sources of different sensory origins, and to what extent sensory-evoked climbing fibre responses depend on the strength and recent history of activation. Here we imaged complex spike responses in cerebellar lobule crus 1 to various types of sensory stimulation in awake mice. We find that different sensory modalities and receptive fields have a mild, but consistent, tendency to converge on individual Purkinje cells, with climbing fibres showing some degree of input-specificity. Purkinje cells encoding the same stimulus show increased events with coherent complex spike firing and tend to lie close together. Moreover, whereas complex spike firing is only mildly affected by variations in stimulus strength, it depends strongly on the recent history of climbing fibre activity. Our data point towards a mechanism in the olivo-cerebellar system that regulates complex spike firing during mono- or multi-sensory stimulation around a relatively low set-point, highlighting an integrative coding scheme of complex spike firing under homeostatic control.

(Received 6 November 2018; accepted after revision 20 March 2019; first published online 25 March 2019)

Corresponding author Laurens Bosman: PO Box 2040, 3000 CA Rotterdam, The Netherlands. Email: l.bosman@erasmusmc.nl; or Tycho Hoogland, PO Box 2040, 3000 CA Rotterdam, The Netherlands. Email: t.hoogland@erasmusmc.nl

Introduction

The olivo-cerebellar system is paramount for sensorimotor integration during motor behaviour. The climbing fibres that originate in the inferior olive and cause complex spike firing in cerebellar Purkinje cells encode both unexpected and expected sensory events and affect initiation, execution as well as adaptation of movements (Albus, 1971; Welsh *et al.* 1995; Kitazawa *et al.* 1998; Gibson *et al.* 2004; Bosman *et al.* 2010; Yang & Lisberger, 2014; Ohmae & Medina, 2015; Ten Brinke *et al.* 2015; Streng *et al.* 2017; Apps *et al.* 2018; Herzfeld *et al.* 2018; Junker *et al.* 2018). Complex spike firing frequency is typically sustained around 1 Hz and is not substantially affected by the behavioural state, although short-lived increases or decreases in firing occur (Bloedel & Ebner, 1984; Mukamel *et al.* 2009; Bosman *et al.* 2010; Rahmati *et al.* 2014; Zhou *et al.* 2014; Hoogland *et al.* 2015; Negrello *et al.* 2019). To date, the paradox between the persistence of complex spike firing and the behavioural relevance of individual complex spikes remains largely unresolved.

Whereas the afferents of Purkinje cells, including not only the climbing fibres but also the parallel fibres and axons of interneurons, all diverge, their efferents strongly converge upon the cerebellar nuclei, ultimately integrating many different inputs from the brain (Harvey & Napper, 1991; Sugihara *et al.* 2001; Person & Raman, 2011). The parallel fibres are oriented in a transverse direction along the lobular axes, while the climbing fibres and axons of the interneurons run perpendicularly to them in line with the sagittal orientation of the dendritic trees of Purkinje cells (Andersen *et al.* 1964; Szentágothai, 1965; Sugihara *et al.* 1999, 2009; Sullivan *et al.* 2005; Gao *et al.* 2006; Ruigrok, 2011; Cerminara *et al.* 2015; Apps *et al.* 2018). Interestingly, the intrinsic biochemical nature as well as

the electrophysiological profile of individual Purkinje cells follows the organization of the climbing fibres so that Purkinje cells located in the same sagittal module receive climbing fibre input from the same olivary subnucleus and have similar identity properties, setting them apart from Purkinje cells in neighbouring modules (Xiao *et al.* 2014; Zhou *et al.* 2014; Cerminara *et al.* 2015; De Zeeuw & Ten Brinke, 2015; Tsutsumi *et al.* 2015; Suvrathan *et al.* 2016). Accordingly, Purkinje cell responses following electrical stimulation of major nerves of cat limbs largely adhere to the parasagittal organization of the climbing fibre zones (Oscarsson, 1969; Groenewegen *et al.* 1979), which in turn can be further differentiated into smaller microzones based upon their response pattern to tactile stimulation of a particular spot on the body (Ekerot *et al.* 1991; Apps & Garwicz, 2005; Ozden *et al.* 2009; De Zeeuw *et al.* 2011). Possibly, differential sensory maps even occur at the sub-microzonal or even at the individual Purkinje cell level, but to our knowledge this has not yet been investigated. In particular, it remains unclear to what extent different types of sensory input can drive complex spikes within the same individual Purkinje cells and/or their direct neighbours and how the strength as well as the history of these inputs influences the distribution of climbing fibre activity.

Here, we studied the impact of minimal stimuli of distinct sensory modalities on complex spike firing of Purkinje cells in crus 1 of awake mice using *in vivo* two-photon Ca^{2+} imaging with Cal-520 (Tada *et al.* 2014). This fluorescent sensor has been reported to track fast-rising calcium transients more faithfully than commonly used genetically encoded sensors such as GCaMP6f (Lock *et al.* 2015). We found that different sensory streams appear to converge on individual inferior olivary neurons and thereby Purkinje cells, that sensory stimulation primarily affects the timing of the complex

spikes rather than their rate, that the strength of complex spike responses varied seamlessly from non-responsive to highly responsive, that a recent history of high activity leads to a future of low activity, and that Purkinje cells that respond to the same stimulus tend to be located in each other's vicinity and display increased levels of simultaneous firing. Together, our data indicate that subtle and local sensory inputs can recruit mosaic ensembles of Purkinje cells, employing population coding in a spatially and temporally dynamic way that is in line with homeostatic control.

Methods

Ethical approval

All experimental procedures involving animals were in agreement with Dutch and European legislation and guidelines as well as with the ethical principles of *The Journal of Physiology*. The experiments were approved in advance by an independent ethical committee (DEC Consult, Soest, the Netherlands) as required by Dutch law and filed with approval numbers EMC2656, EMC3001 and EMC3168. Experiments were performed in compliance with the guidelines of the Animal Welfare Board of the Erasmus MC.

Animals and surgery

Mice were group housed until the day of the experiment and kept under a regime with 12 h light and 12 h dark with food and water available *ad libitum*. The mice had not been used for other experiments prior to those described here.

For the experiments performed in awake mice, we recorded from in total 66 fields of views located in cerebellar lobule crus 1 of 29 male C57BL/6J mice of 4–12 weeks of age (Charles Rivers, Leiden, the Netherlands). Prior to surgery, mice were anaesthetized using isoflurane (initial concentration: 4%, v/v, in O₂, maintenance concentration: ca 2%, v/v) and received Carprofen (Rimadyl, 5 mg/ml s.c.) to reduce post-surgical pain. Before the start of the surgery, the depth of anaesthesia was verified by the absence of a reaction to an ear pinch. To prevent dehydration, mice received 1 ml of saline s.c. injection before the surgeries commenced. Eyes were protected using eye ointment (Duratears, Alcon, Fort Worth, TX, USA). Body temperature was maintained using a heating pad in combination with a rectal thermometer. During surgery, we attached a metal head plate to the skull with dental cement (Superbond C&B, Sun Medical Co., Moriyama City, Japan) and made a craniotomy with a diameter of approximately 2 mm centred on the medial part of crus 1 ipsilateral to the side of somatosensory stimulation. The dura mater was preserved

and the surface of the cerebellar cortex was cleaned with extracellular solution composed of (in mM) 150 NaCl, 2.5 KCl, 2 CaCl₂, 1 MgCl₂ and 10 Hepes (pH 7.4, adjusted with NaOH). After surgery, the mice were allowed to recover from anaesthesia for at least 30 min. Subsequently, the mice were head-fixed in the recording setup and they received a bolus-loading of the Ca²⁺ indicator Cal-520 (0.2 mM; AAT Bioquest, Sunnyvale, CA, USA) (Tada *et al.* 2014). Cal-520 was used as it is currently the best available green Ca²⁺ dye, outperforming genetically encoded indicators such as GCaMP6f (Lock *et al.* 2015). The dye was first dissolved with 10% w/v Pluronic F-127 in DMSO (Invitrogen, Thermo Fisher Scientific, Waltham, MA, USA) and then diluted 20 times in the extracellular solution. The dye solution was pressure injected into the molecular layer (50–80 μm below the surface) at 0.35 bar for 5 min. Finally, the brain surface was covered with 2% agarose dissolved in saline (0.9% NaCl) in order to reduce motion artefacts and prevent dehydration.

For the experiments on single-whisker stimulation we made recordings under anaesthesia on 17 male C57BL/6J mice of 4–12 weeks of age. The procedure was largely the same as described above, but instead of isoflurane we used ketamine/xylazine as anaesthetic (i.p. injection via butterfly needle, initial dose: 100 and 10 mg/kg, respectively; maintenance dose: approximately 60 and 3 mg/kg/h, respectively). The mice remained under anaesthesia until the end of the recording. A subset of these experiments was performed with 0.2 mM Oregon Green BAPTA-1 AM dye (Invitrogen) as this dye has been more widely used than Cal-520 (e.g. Stosiek *et al.* 2003; Ozden *et al.* 2009; Schultz *et al.* 2009; Hoogland *et al.* 2015). Oregon Green BAPTA-1 AM was dissolved and applied in the same way as Cal-520. We found that Cal-520 had a superior signal-to-noise ratio under our experimental conditions. As a consequence, the observed event rate was lower in the experiments using OGB-1 (OGB-1: 0.45 ± 0.26 Hz; *n* = 172 cells; Cal-520: 0.72 ± 0.40 Hz; *n* = 43 cells; median ± interquartile range; *U* = 1719.0, *P* < 0.001, Mann–Whitney test). The observed frequency range using Cal-520 was comparable to that found using *in vivo* single-unit recordings under ketamine/xylazine anaesthesia: 0.6 ± 0.1 Hz (Bosman *et al.* 2010). Despite an underestimation of the complex spike rate using OGB-1, we found that the ratios of Purkinje cells that responded to single whisker stimulation were similar for both dyes [OGB-1: 89 out of 373 cells (24%); Cal-520: 35 out of 152 cells (23%); *P* = 0.910; Fisher's exact test]. We therefore combined the data from both dyes. For the analysis presented in Fig. 11, we included only those cells that could be recorded during all stimulus conditions. All experiments using awake data were obtained with Cal-520.

At the end of each experiment, the mice were killed by cervical dislocation under isoflurane or ketamine/xylazine

anaesthesia after which the brain was removed and the location of the dye injection in crus 1 was verified by epifluorescence imaging. The whole procedure, from initial anaesthesia to cervical dislocation, typically lasted around 6–8 h.

In vivo two-photon Ca²⁺ imaging

Starting at least 30 min after dye injection, *in vivo* two-photon Ca²⁺ imaging of the molecular layer of crus 1 was performed using a setup consisting of a Ti:sapphire laser (Chameleon Ultra, Coherent, Santa Clara, CA, USA), a TriM Scope II system (LaVisionBioTec, Bielefeld, Germany) mounted on a BX51 microscope with a 20 \times , 1.0 NA water immersion objective (Olympus, Tokyo, Japan) and GaAsP photomultiplier detectors (Hamamatsu, Iwata City, Japan). A typical recording sampled a field of view of 40 \times 200 μ m with a frame rate of approximately 25 Hz.

In a subset of experiments (Fig. 12A–C), larger fields-of-view were obtained using a two-photon setup from Neurolabware (Los Angeles, CA, USA). Imaging occurred through a 16 \times (0.8 NA) objective (Nikon, Tokyo, Japan) in combination with a Chameleon Ultra II laser (Coherent) tuned to 920 nm at a frame rate of 15 Hz.

Sensory stimulation

Cutaneous stimuli were delivered to four defined regions on the left side of the face, ipsilateral to side of the craniotomy. These regions were the whisker pad, the cheek posterior to the whisker pad, the upper lip and the lower lip. Stimuli were applied using a Von Frey filament (Touch Test Sensory Evaluator 2.83, Stoelting Co., IL, USA) attached to a piezo linear drive (M-663, Physik Instrumente, Karlsruhe, Germany). Prior to the set of experiments described here, we tested a series of eight Von Frey filaments with a stiffness range from 0.02 to 1.4 g in awake head-fixed mice to select the optimal force for these experiments. We selected the 0.07 g (0.686 mN) filament because this filament induced a mild reaction in the mouse, but no signs of a nociceptive response (cf. Chaplan *et al.* 1994). The touch time was fixed at 100 ms. As a control, we moved the stimulator without touching the face ('sound only' condition). Visual stimuli were delivered as 10 ms pulses using a 460 nm LED (L-7104QBC-D, Kingbright, CA, USA). The stimulation frequency was fixed at 1 Hz and the different stimuli were applied in a random order. Video recordings of the eye, made under infrared illumination, revealed that the mice did not make eye movements in response to the LED flash, but they did show reflexive pupil constriction (data not shown).

Single whiskers were stimulated using a piezo linear drive (M-663, Physik Instrumente) while using a deflection of 6°. It took the stimulator approximately 30 ms to reach this position. At the extreme position, the

stimulator was paused for 150 ms before returning to the neutral position. The stimulator was designed to minimize contact with other whiskers. Each stimulation experiment consisted of five sessions in random order. During each block, one of the ipsilateral whiskers B2, C1, C2, C3 and D2 was stimulated. Each session consisted of 150 stimuli at 2 or 3 Hz.

Complex spike detection

Image analysis was performed offline using custom made software as described and validated previously (Ozden *et al.* 2008, 2012; De Gruijl *et al.* 2014). Briefly, independent component analysis was applied to the image stack to discover masks describing the locations of individual Purkinje cell dendrites (e.g. see Fig. 2A). For each field of view, the mask was generated only once, so that the same Purkinje cells were analysed for subsequent recordings of different stimulus conditions, enabling paired comparisons. Experiments during which spatial drift occurred were discarded from subsequent analysis. The fluorescence values of all pixels in each mask were averaged per frame. An 8% rolling baseline from a time window of 0.5 ms was subtracted from the average fluorescence per mask (Ozden *et al.* 2012), after which Ca²⁺ transient events were detected using template matching.

Statistical analysis

In general, we first tested whether parameter values were distributed normally using one-sample Kolmogorov–Smirnov or Shapiro–Wilk tests. If not, non-parametric tests were applied. When multiple tests were used, Benjamini–Hochberg correction for multiple comparisons was applied. For each experiment, stimuli were given in a random sequence. Identification of Purkinje cell dendrites and event extraction were performed by a researcher who was blind to the type of stimulus. For the experiments characterizing response characteristics of individual Purkinje cells, we compared the fraction of responsive Purkinje cells, the response latency and the response peak. After extracting the Ca²⁺ transient event times, peri-stimulus time histograms (PSTHs) were constructed using the inter-frame time (approximately 40 ms) as bin size. Stacked line plots of Purkinje cell PSTHs were sorted by weak to strong peak responses. The data were normalized such that the top represents the average responses of all Purkinje cells. Statistical significance of responses occurring within 200 ms from stimulus onset was evaluated using a threshold of the mean + 3 SD of the firing rate during the 500 ms prior to stimulus onset (300 ms for the single whisker stimulation experiments, as they were performed with a higher stimulation frequency).

To calculate whether two or more inputs converged on single Purkinje cells we used a bootstrap method. First, we determined the fraction of responsive cells for each parameter and compared these to a randomly generated number between 0 and 1 as taken from a uniform distribution. If for each input the randomly generated numbers were lower than the measured fractions, we considered them as responsive to all stimuli. This procedure was repeated 10,000 times and the mean and standard deviation were derived and used to calculate the Z score of the experimental data. All bootstrap procedures were performed using custom-written code in LabVIEW (National Instruments, Austin, TX, USA).

A direct comparison between the full and partial correlations of the peak responses to tactile stimuli was performed in MATLAB (MathWorks, Natick, MA, USA) (see Fig. 8A, B). Principal component analysis of the same dataset was also performed in MATLAB and compared to that of a bootstrapped dataset (Fig. 8C). The latter was obtained by shuffling, for each stimulus condition, the peak responses of each Purkinje cell 500 times. In this way, we maintained the obtained peak responses, but distributed them randomly and independently for all stimulus conditions over all Purkinje cells. After each shuffle, a principal component analysis was performed and finally the mean (± 3 SD) of these principal component analyses was calculated and plotted. The analyses described in Fig. 8A–C were performed on those 188 Purkinje cells that received all four tactile stimuli. For the principal component analysis we used a 4×188 matrix of Z-scored response amplitudes.

The distributions of pairs of Purkinje cells, either both statistically significantly responsive to a given stimulus ('responsive pairs') or one cell being responsive and the other not ('heterogeneous pairs'), were tested using two-dimensional Kolmogorov–Smirnov tests performed in MATLAB. Aggregate PSTHs (Fig. 13) were constructed and evaluated as described before (Romano *et al.* 2018). Briefly, we calculated per individual frame the number of simultaneously occurring events and colour coded these in a PSTH combining data from all dendrites in a field of view. Based upon the total number of complex spikes and dendrites per recording, we calculated the expected number of simultaneous complex spikes per individual frame using a Poisson distribution. The actual number of simultaneous complex spikes was compared to this calculated distribution and a P value was derived for each number based upon the Poisson distribution (using custom-written software in MATLAB and LabVIEW). Unless mentioned otherwise, correlation analysis was performed in SigmaPlot (Systat Software, San Jose, CA, USA) and the other statistical tests were performed using SPSS (IBM, Armonk, NY, USA).

Results

Climbing fibre responses to tactile, auditory and/or visual input

Little is known about the distribution and convergence of different types of climbing fibre-mediated sensory input at the level of individual, nearby Purkinje cells. Here, we performed two-photon Ca^{2+} imaging of Purkinje cells of awake mice to record complex spike responses to various types of sensory stimulation related to the face of the mice. The recordings were made in crus 1 as this lobule is known to receive sensory input from the oro-facial region, in particular from the mystacial vibrissae (Fig. 1A) (Shambes *et al.* 1978; De Zeeuw *et al.* 1990; Yatim *et al.* 1996; Apps & Hawkes, 2009; Bosman *et al.* 2011; De Gruijl *et al.* 2013; Kubo *et al.* 2018; Romano *et al.* 2018). The configurations and positions of individual Purkinje cell dendrites were detected using independent component analysis (Fig. 1B). Ca^{2+} transients were isolated per dendrite by a template-matching procedure that reliably detects complex spikes (Ozden *et al.* 2008; De Gruijl *et al.* 2014; Najafi *et al.* 2014) (Fig. 1C–E).

We started our study of sensory responses by using air puff stimulation of the large facial whiskers, which is a relatively strong stimulus. In line with previous studies (Axelrad & Crepel, 1977; Brown & Bower, 2002; Bosman *et al.* 2010; Apps *et al.* 2018; Romano *et al.* 2018), we found that air puff stimulation to the whiskers evoked complex spike responses in many Purkinje cells (e.g. in 19 out of 19 Purkinje cells in the example illustrated in Fig. 2). In total, 102 out of the 117 (87%) cells analysed were considered to be responsive to such a stimulus, implying that the peak responses of these cells exceeded the threshold of the mean $+ 3$ SD of the pre-stimulus period.

Complex spikes are associated with a fast and large increase in intracellular Ca^{2+} in the dendrites of Purkinje cells, but other processes may also contribute to a rise in the intracellular Ca^{2+} concentration (Najafi *et al.* 2014; Roome & Kuhn, 2018). Indeed, in our data, we observed changes in fluorescence that were not related to complex spikes (Fig. 2H). To exclude the possibility that we erroneously detected such non-complex spike events as complex spikes, we overlaid trials with and without complex spikes. This revealed that fluorescence events that were not classified as complex spikes typically had smaller amplitudes and slower kinetics than complex spikes, with the exception of a very noisy recording where non-complex spikes were much faster than complex spikes (Fig. 3A). This confirms the impression revealed in Fig. 1D and E that complex spikes can be properly detected based upon their waveform, in line with previous reports using the same detection algorithm (Ozden *et al.* 2008; De Gruijl *et al.* 2014; Najafi *et al.* 2014). To further characterize the rise times, we performed a set of

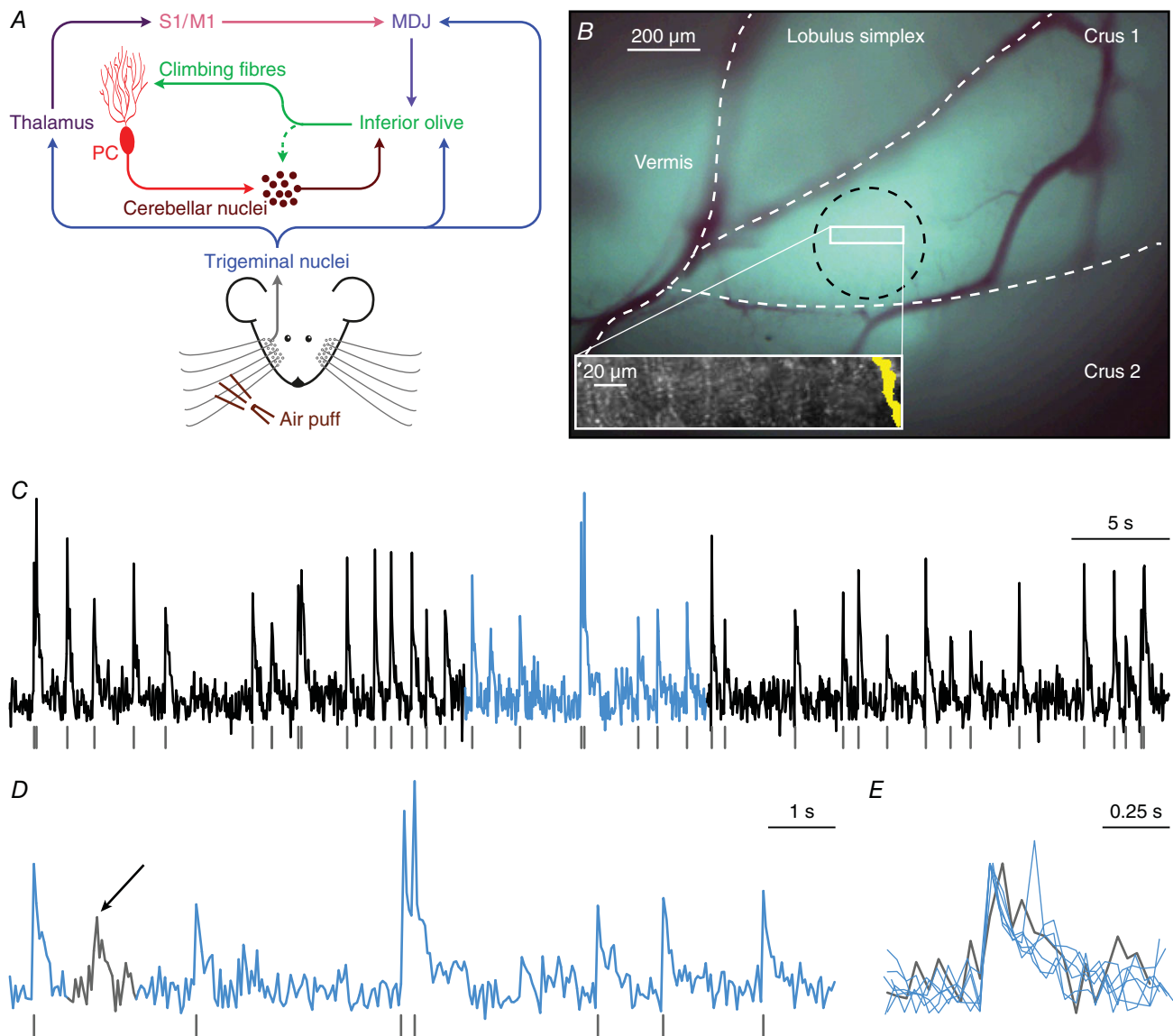


Figure 1. Sensory pathways carrying facial input to the cerebellar cortex

A, scheme of the main routes conveying facial tactile input via the climbing fibre pathway to cerebellar Purkinje cells (PC). Climbing fibres, which cause complex spike firing in Purkinje cells, exclusively originate from the inferior olive. The inferior olive, in turn, is directly innervated by neurons from the trigeminal nuclei as well as indirectly via thalamo-cortical pathways that project to the inferior olive mainly via the nuclei of the mesodiencephalic junction (MDJ). The MDJ itself also receives direct input from the trigeminal nuclei. See main text for references. B, *in vivo* two-photon Ca^{2+} imaging was performed to characterize Purkinje cell complex spike responses to sensory stimulation in the medial part of crus 1. Purkinje cells were detected using independent component analysis and the position of a Purkinje cell dendrite (yellow area on the right) within a field of view is shown in the inset. At the end of each recording session, the brain was removed and the location of the dye injection in medial crus 1 was confirmed through *ex vivo* epifluorescence imaging (black circle). The white rectangle indicates the approximate recording location. C, complex spikes that were triggered by climbing fibre activity were retrieved from fluorescence traces of individual Purkinje cells. A representative trace obtained from the Purkinje cell dendrite illustrated in B is shown together with the detected complex spikes (grey lines). The light blue episode is enlarged in D. Complex spikes were detected by the combination of a threshold and a template matching algorithm. Only events with a sharp rising phase were accepted as complex spikes. In the 60 s interval shown in C, there was one event with a slower rise time (see arrow in D), as indicated at a larger time scale in E. The events in E are scaled to peak.

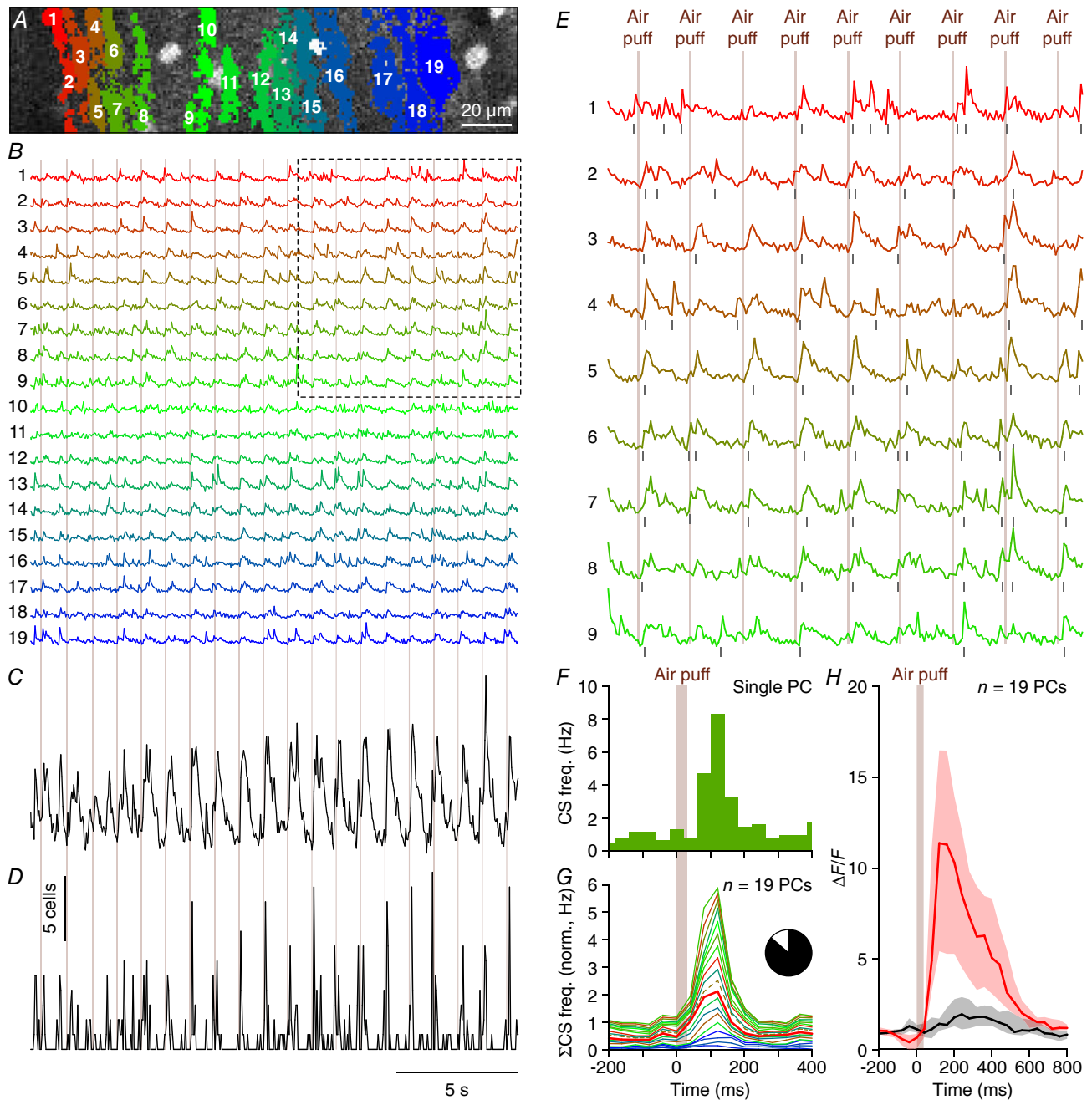


Figure 2. Whisker stimulation evokes complex spike responses in cerebellar crus 1
 A, complex spikes elicit large increases in the Ca^{2+} concentration within Purkinje cell dendrites that can be resolved using *in vivo* two-photon microscopy in combination with a fluorescent Ca^{2+} indicator. An example of a field of view with 19 identified Purkinje cell dendrites located in the medial part of crus 1 is shown with each individual dendrite denoted by a number and a unique colour. This recording was made in an awake mouse. B, fluorescence traces of each of these dendrites show distinct Ca^{2+} transient events, which are to a large extent associated with air puff stimulation of the facial whiskers (times of stimulation indicated by vertical lines). The boxed area is enlarged in E. C, summed fluorescence trace composed of all 19 individual traces emphasizing the participation of many Purkinje cells to the stimulus-triggered responses. D, after complex spike extraction, a clear relationship between stimulus and activity was observed as illustrated by summing, for each frame, the number of complex spikes observed over all dendrites. The vertical scale bar corresponds to the simultaneous activity of five Purkinje cells. E, enlargement of the boxed area in B. The air puffs were delivered once every second. F, peri-stimulus time histogram of a Purkinje cell dendrite (marked as number 7 in A and B) in response to air puff stimulation to the ipsilateral whiskers (154 trials). The bin size (40 ms) corresponds to the acquisition frame rate (25 Hz). G, normalized stacked line graph of the Purkinje cells in this field of view showing that every cell contributed to the

experiments with a smaller field of view and a higher frame rate (100 Hz). These recordings revealed that virtually all events had a rise time of one or two frames (10 or 20 ms) (Fig. 3B–D).

To address whether localized and more subtle stimuli recruited smaller groups of Purkinje cells, perhaps even subsets of microzones, we subsequently applied gentle tactile stimulation at four facial locations: the whisker pad, the cheek posterior to the whisker pad, the upper lip and the lower lip (Fig. 4A). Although the precise somatotopy of climbing fibre projections to crus 1 is not known, it has been shown that the mossy fibre projections to crus 1 convey somatosensory input mainly from the mystacial vibrissae and the surrounding skin, while the somatosensory input from the lips predominantly targets crus 2 (Shambes *et al.* 1978). The stimuli were given using a Von Frey filament (target force = 0.686 mN) attached to a piezo actuator. Stimulus strength was carefully calibrated to avoid inducing responses from neighbouring skin areas or nociceptive responses (see Methods). The strength of the Purkinje cell responses to any of the four tactile stimuli (998 stimulus conditions in 282 Purkinje cells) had a skewed, but continuous distribution (Fig. 4B). Moreover, for individual stimulus locations such skewed distributions of response strengths were found as well, with the upper lip being the least sensitive of the four facial areas (Fig. 5). In other words, our dataset contained a gradient of both non-responsive and strongly responsive Purkinje cells. A distinction between ‘responsive’ and ‘non-responsive’ Purkinje cells therefore involved a somewhat arbitrary distinction, prompting us to present most of the subsequent analyses using the entire dataset.

Given that touches were delivered by a piezo-actuator that made a weak but audible sound, we also tested whether Purkinje cells responded to this sound in the absence of touch. This was the case, and, as expected, the ‘sound-only’ stimulus evoked the weakest responses of all stimuli ($P < 0.001$; Kruskal–Wallis test; Fig. 5B). For comparison, we also included a visual stimulation, consisting of a brief (10 ms) flash of a blue LED. This stimulus evoked responses with a similar strength as the whisker pad and lower lip stimulation, but with a latency that was remarkably long (Fig. 5A).

To facilitate a quantitative comparison between the stimulus conditions, we subsequently focused on the subset of obvious responses, defined as having a peak amplitude exceeding our threshold for significance set at the average + 3 SD of the pre-stimulus period. Among these ‘significantly responding’ Purkinje cells, we found trends as in the entire population: the lower lip recruited the strongest responses, directly followed by the whisker pad and visual stimulation, while upper lip and sound-only stimulations were less effective (Fig. 4C–E; Table 1). We also confirmed the remarkably long latency, typically more than 100 ms, for the visually evoked responses ($P < 0.001$ compared to the tactile stimuli; Kruskal–Wallis test; Fig. 4F; Table 1).

Convergence of sensory inputs

Next, we addressed the question of whether Purkinje cells have a preference to respond to one or multiple types of stimulation. To this end, for each combination of two stimuli we made a scatter plot of the response strengths of each individual Purkinje cell. For each and every combination, correlation analysis revealed a positive correlation, implying that a stronger response to one stimulus typically implied also a stronger response to the other (Fig. 6A). These correlations, although weak, were statistically significant for all combinations except in two cases (i.e. upper lip vs. sound-only and upper lip vs. visual stimulation; Table 2). The regression lines deviated from the 45° line, suggesting that, although there is a tendency at the population level to combine inputs, individual Purkinje cells can display specificity for a given stimulus. The Venn diagrams in Fig. 6B and C highlight the degree of overlap for all combinations of two and three stimuli. For all combinations we found some but not complete overlap. Remarkably, when comparing the observed overlap with the expected overlap based upon a random distribution, all combinations occurred more often than predicted. To test to what extent the observed overlaps were statistically significant, we performed a bootstrap analysis (see Methods) and this indicated that, indeed, most overlaps occurred significantly more often than expected from a random distribution of inputs (Fig. 6B and C, Tables 3 and 4). This also included the visual stimulation, so that those Purkinje cells responding to a

overall response. The Purkinje cells are ranked by their maximal response and the data are normalized so that the top line reflects the average frequency per bin. Cell no. 5 (dashed line) had a relatively poor signal-to-noise ratio during later parts of the recording (see Fig. 3), but it had nevertheless a complex spike response profile that was indistinguishable from the other cells. The colours match those in A and B. Inset: in total, 102 out of 117 cells analysed (87%) were responsive to whisker air puff stimulation (peak response exceeded average + 3 SD of the pre-stimulus interval). H, median fluorescence traces of the trials with (red) and without (black) complex spikes fired during the first 200 ms after air puff onset. In the absence of complex spike firing, only a very small increase in fluorescence was observed, indicating that most of the change in fluorescence was associated with complex spike firing. Note the longer time scale than in F and G. The lines indicate the medians and the shaded areas the interquartile ranges of the 19 Purkinje cells in this field of view.

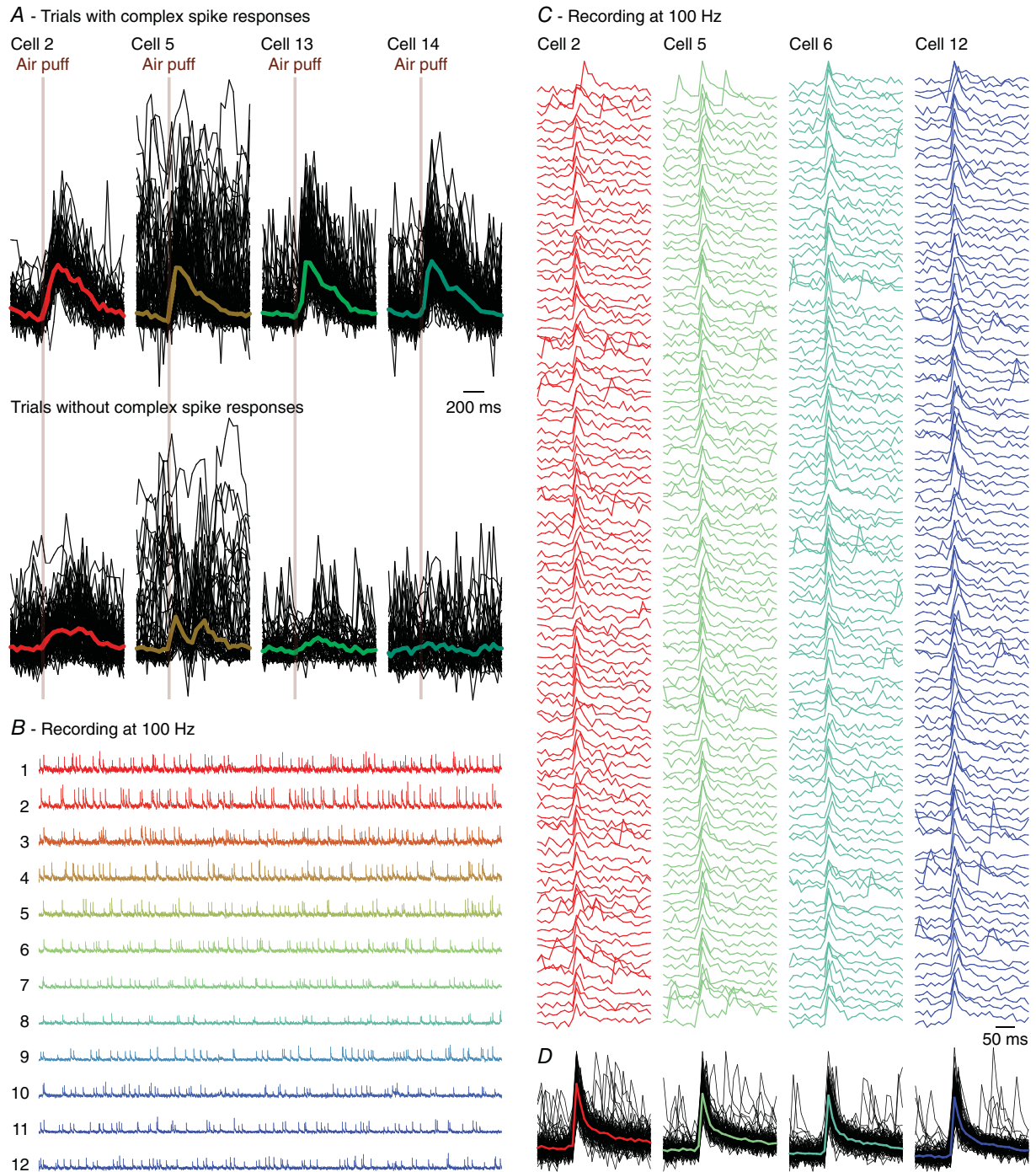


Figure 3. Complex spike detection

A, from the same experiment as illustrated in Fig. 2, we randomly selected four Purkinje cells of which all trials with (top) and without (bottom) a complex spike within 200 ms of stimulus onset are shown. The signals are scaled to the maximum of the median complex spike responses. The fat coloured lines indicate the medians, with the same colour code as in Fig. 2. Trials without a complex spike response can still show increased fluorescence, but the kinetics of the non-complex spike response differed from those of the complex spike responses. Note that the raw trace of cell 5 had a period with increased noise levels, making it the least reliable cell of this recording. Nevertheless, cell 5 had a complex spike response profile that was very similar to those of the other cells (see dashed line in Fig. 2G). Cells (in other recordings) that had a signal-to-noise ratio worse than for cell 5 of this recording were excluded from analysis. B, to better characterize rise times, we made recordings with a smaller field of view, but a higher temporal resolution (100 Hz). Shown are 60 s traces of 12 simultaneously recorded Purkinje cells. C, of four randomly selected Purkinje cells, the first 100 events were plotted and superimposed (D). The coloured lines in D indicate the medians. Virtually all events had a rise time of 10 or 20 ms (one or two frames).

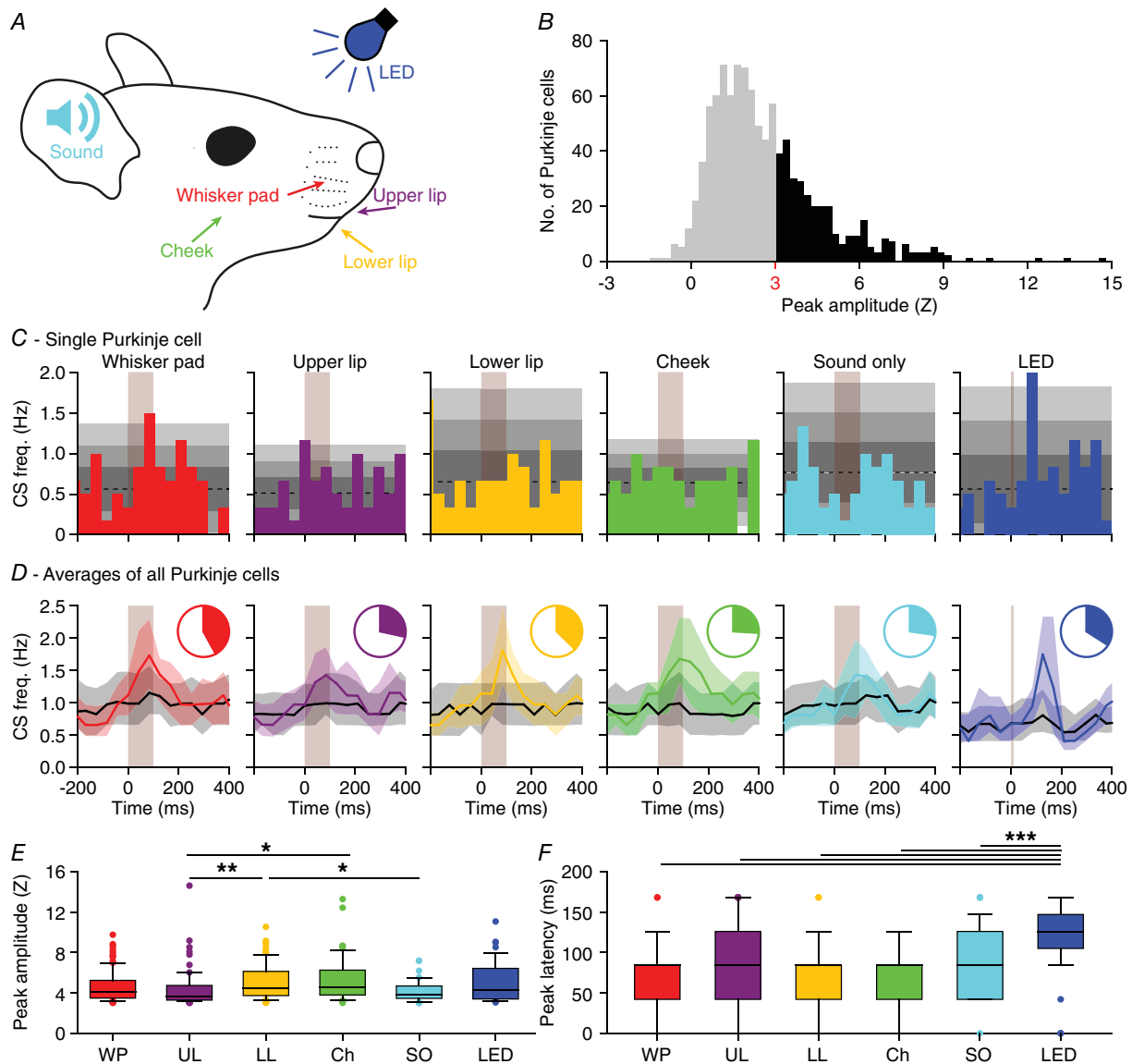


Figure 4. Purkinje cells in crus 1 respond to various types of sensory stimulation

A, tactile stimuli were presented to four facial regions in awake mice: the whisker pad (WP), the upper lip (UL), the lower lip (LL) and the cheek (Ch). Each stimulus was delivered with a piezo-actuator that made a muted, yet audible sound which was also delivered without touch ['sound only (SO)']. A blue light flash generated by an LED was used as the visual stimulus. These experiments were performed in awake mice. B, to avoid interference of adjacent areas, we applied gentle touches (0.686 mN). The complex spike response ratio was much reduced relative to the strong air puff stimulation to all ipsilateral whiskers illustrated in Fig. 2. A histogram of the peak responses (expressed as Z value) of all responses to either of the four tactile stimuli demonstrates that the response strength is a continuum, showing the lack of a clear separation between 'responsive' and 'non-responsive' Purkinje cells (998 stimulus conditions in 282 Purkinje cells). We considered Purkinje cells that showed a peak response above $Z = 3$ as 'significantly responsive' (represented with black bars), but we provide most of the analyses also for the population as a whole (e.g. Fig. 5). C, peri-stimulus time histograms (PSTHs) of a representative Purkinje cell. The shades of grey indicate 1, 2 and 3 SD around the average. Each stimulus was repeated 154 times at 1 Hz. D, for every stimulus condition, we averaged the PSTHs for all Purkinje cells that were significantly responsive to that particular stimulus [coloured lines; medians (interquartile range)]. These were contrasted to the averaged PSTH of the other Purkinje cells (black lines). The pie charts represent the fraction of Purkinje cells significantly responsive to a particular stimulus. See also Table 1. E, peak responses of the significantly responding Purkinje cells were lowest for sound-only and for upper lip stimulation. $*P < 0.05$; $**P < 0.01$ (post hoc tests after Kruskal–Wallis test). F, as expected for complex spike responses to weak stimulation, the latencies were relatively long and variable, but consistent across types of stimulation. Only visual stimulation (LED) had a remarkably longer latency time. $***P < 0.001$ (post hoc tests after Kruskal–Wallis test for LED vs. whisker pad, upper lip, lower lip and cheek and $P < 0.05$ compared to sound only).

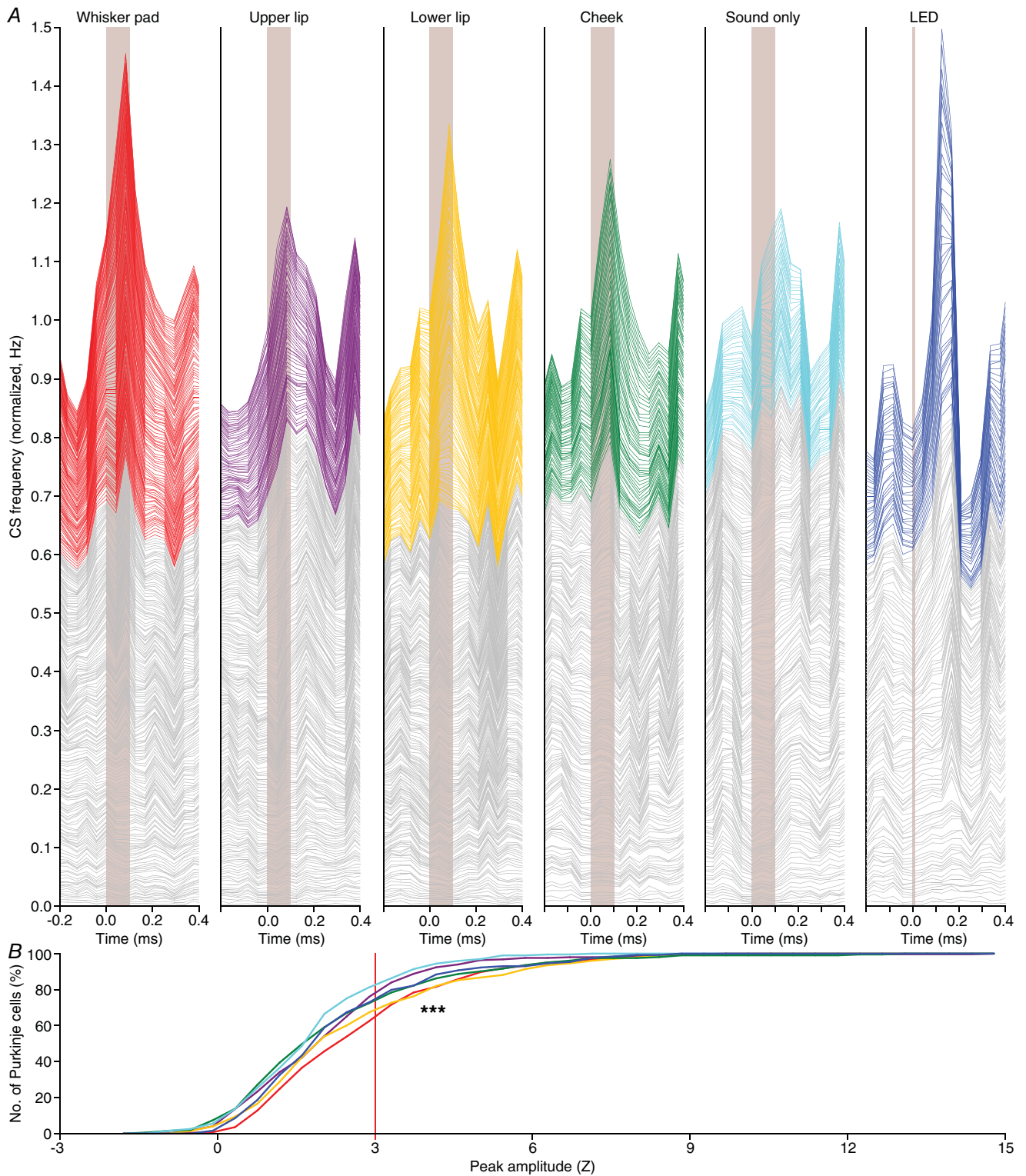


Figure 5. Variations in response strength

A, stacked line plots illustrating the peri-stimulus time histograms of all Purkinje cells recorded under either of the six indicated stimulus conditions. The cells are ordered based upon their peak responses (calculated as Z value) during the 200 ms interval following stimulus onset, with the cell with the lowest response at the bottom of each graph. The grey lines indicate cells with a peak response deemed not significant ($Z < 3$) and the coloured lines indicate the significant responses ($Z > 3$). The graphs are normalized so that the upper line depicts the average of all cells. As shown in Fig. 4B, we cannot discriminate between responsive and non-responsive cells in an all-or-none

Table 1. Purkinje cell responses to sensory stimulation in awake mice

Stimulation	Responsive cells		Response parameters		Significance (<i>P</i>) $\chi^2 = 25.758$; d.f. = 5; <i>P</i> = 0.001				
	No.	%	Peak (Hz)	Latency (ms)	UL	LL	Ch	SO	LED
Whisker pad	111 (282)	39	2.12 ± 0.82	84 ± 42	0.010	0.661	0.003	0.000	0.828
Upper lip	71 (249)	29	1.89 ± 0.67	84 ± 84		0.031	0.597	0.157	0.064
Lower lip	99 (264)	38	2.23 ± 0.97	84 ± 42			0.010	0.001	1.000
Cheek	53 (203)	26	2.30 ± 1.67	84 ± 42				0.415	0.028
Sound only	44 (197)	22	1.74 ± 0.65	84 ± 84					0.003
LED	49 (129)	34	2.13 ± 1.18	126 ± 0					

Purkinje cells respond with complex firing to sensory stimulation (Fig. 4). For each type of stimulation, the number and percentage of statistically significantly responsive cells (peak response > average + 3 SD of baseline firing) is indicated (in parentheses: total number of cells tested). The response peak and response latency are indicated as medians ± interquartile ranges. Some stimuli recruited more Purkinje cells with statistically significant responses than others. The differences in fractions of responsive Purkinje cells were statistically significant ($6 \times 2 \chi^2$ test) and further tested using pair-wise Fisher's exact tests (as the χ^2 test was significant, no further correction for multiple comparisons was applied). Bold numbers indicate statistically significant values. UL = upper lip; LL = lower lip; Ch = cheek; SO = sound only.

tactile stimuli were often responsive to visual stimulation as well.

One might ask whether Purkinje cells in crus 1 encode specific sensory events or, alternatively, respond indifferently to any external trigger. In this context, the response pattern to the sound-only stimulus is especially noteworthy. A weak, but audible sound was generated by the piezo actuator used to deliver the tactile stimuli. Hence, all tactile stimuli also involved sound. Nevertheless, the Venn diagrams in Fig. 6B show that there are Purkinje cells that responded statistically significantly to sound only, but not to sound and touch delivered simultaneously. This could be taken as an argument against the input-specificity of Purkinje cells. However, one should keep in mind that the separation between 'responsive' and 'non-responsive' Purkinje cells is arbitrary (cf. Fig. 4B), and to be able to draw such a conclusion, there should be a consistent absence of preferred responses. The sound-only stimulus was found to be the weakest stimulus (Figs 4E and 5B) and pair-wise comparisons of the response strengths had a bias towards stimuli involving touch (Fig. 6A). This is further illustrated in a single experiment, directly comparing the responses evoked by whisker pad touch and sound-only stimulation. Four randomly selected Purkinje cells from this experiment failed to show a response to sound-only stimuli in the absence of touch responses (Fig. 7A–E). This was confirmed by the group-wise analysis of all Purkinje cells in this experiment, demonstrating a clear

Table 2. Correlations between response probabilities

Stimulation	Pearson correlation (<i>R</i>)				
	Upper lip	Lower lip	Cheek	Sound only	LED
Whisker pad	0.272***	0.253***	0.166*	0.257*	0.358***
Upper lip		0.192**	0.189**	0.130	0.129
Lower lip			0.387***	0.513***	0.339***
Cheek				0.485***	0.362***
Sound only					0.523***

For each Purkinje cell, we made pair-wise comparisons of the Z scores of the response amplitudes to different stimuli. For each pair of stimuli, the Pearson correlation coefficient (*R*) was calculated for the complete population of Purkinje cells subjected to that pair of stimuli. The *P* values of these correlations underwent Benjamini–Hochberg correction for multiple comparisons. These data are graphically represented in Fig. 5A. **P* < 0.05; ***P* < 0.01; ****P* < 0.001.

preference for the whisker pad stimulation over the sound only stimulus (Fig. 7F and G).

Thus, Purkinje cells in crus 1 seem to respond to multiple stimuli, although at the level of individual cells not all stimuli were equally effective in triggering complex spikes. To better disentangle the general responses from input-specific responses, we first focused on the 188 Purkinje cells that received inputs from all four tactile

fashion. Instead, the cells form a continuum that ranges from non-responsive to highly responsive. As this way of plotting relies on the numerical average, a skewed distribution can put emphasis on a relatively small group of cells. The Purkinje cell responses are therefore also compared using cumulative histograms (B) using the same colour scheme as in A. From this representation, it is confirmed that whisker pad and lower lip stimulation yield the strongest responses, while visual stimulation (LED) recruits a few cells with a relatively strong response, increasing the numerical average (see A). Here, we tested the complete distributions (****P* < 0.001; Kruskal–Wallis test). Pair-wise comparisons of all stimulus conditions are presented in Fig. 6.

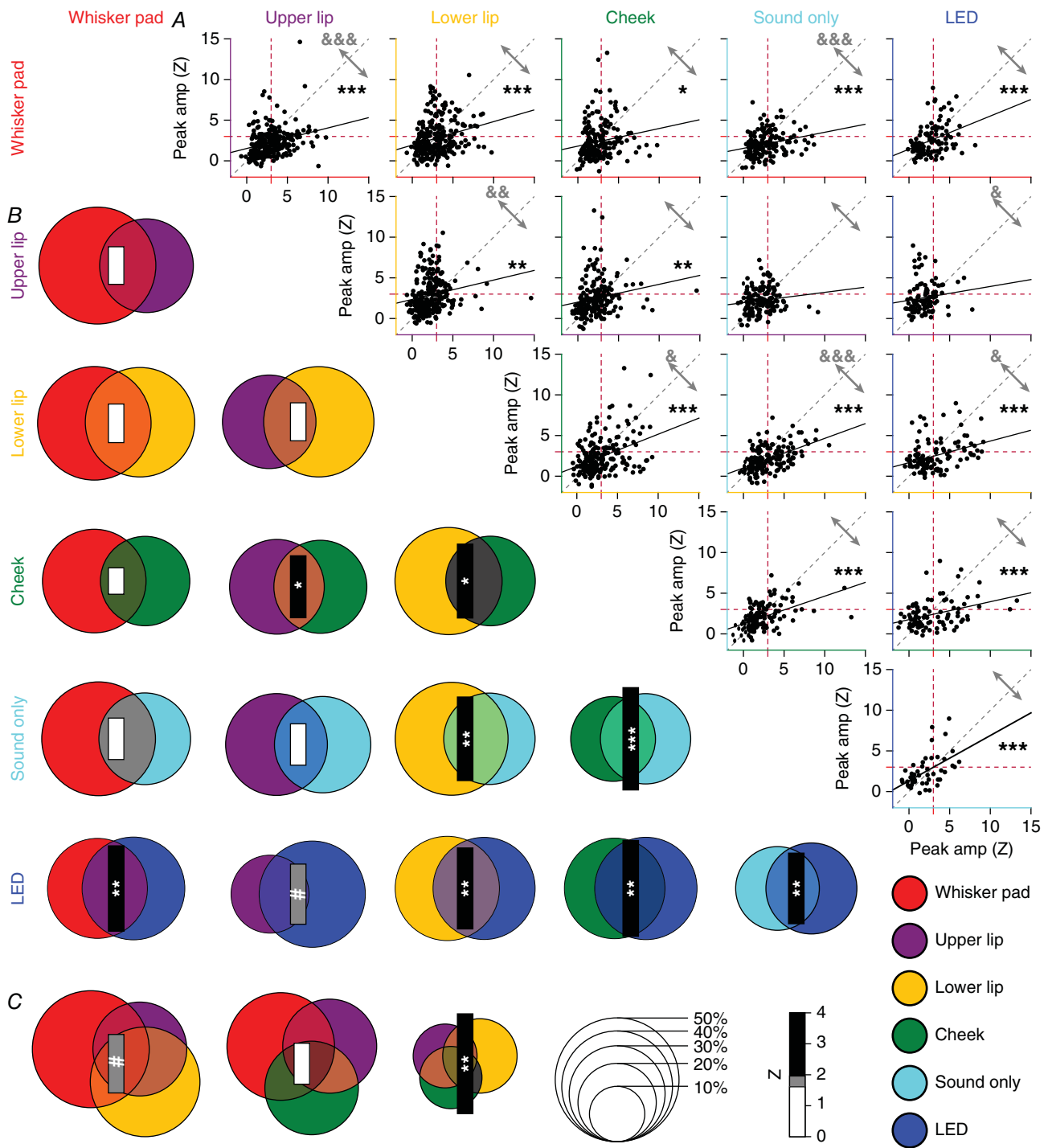


Figure 6. Convergence of sensory input on Purkinje cells

A, to test whether sensory inputs converge on individual Purkinje cells in awake mice, we made pair-wise comparisons of the response amplitudes to two different stimuli per Purkinje cell (scatter plots). For all possible combinations, we found a positive slope of the linear regression analysis. For the majority of combinations, the correlation between response strengths was highly significant: $*P < 0.05$, $**P < 0.01$ and $***P < 0.001$ (Pearson correlation with Benjamini–Hochberg correction for multiple comparisons). Only upper lip and upper lip vs. visual stimulation were not significantly correlated. For this analysis, we included all Purkinje cells, whether they had a statistically significant response or not. The red dotted lines indicate a Z-score of 3, which we set as the threshold for significance (cf. Fig. 4B). They grey arrows indicate the fraction of observations above and below the unity line (grey dotted line). The relative strengths of each stimulus combination were compared in a pairwise fashion (Wilcoxon tests with Benjamini–Hochberg correction for multiple comparisons): $&P < 0.05$, $&&P < 0.01$

Table 3. Convergence of different sensory streams on individual Purkinje cells

Stimulation	Difference from chance (Z)				
	Upper lip	Lower lip	Cheek	Sound only	LED
Whisker pad	1.21	1.25	0.85	1.34	2.75**
Upper lip		1.23	2.00*	1.34	1.94
Lower lip			2.39*	2.70**	2.62**
Cheek				3.31**	3.10**
Sound only					2.28*

For each type of stimulus, we compared the observed rate of convergence on individual Purkinje cells to chance level, using a bootstrap method based on the relative prevalence of responses to each stimulus (cf. Fig. 5). The difference from chance is indicated by Z values. All combinations occurred more often than expected ($Z > 0$). The P values of these correlations underwent Benjamini–Hochberg correction for multiple comparisons. * $P < 0.05$; ** $P < 0.01$.

Table 4. Convergence of different sensory streams on individual Purkinje cells

Stimulation	Difference from chance (Z)
WP + UL + LL	1.89
WP + LL + Ch	1.32
UL + LL + Ch	3.22**
WP + UL + LL + Ch	3.07**

For each type of stimulus, we compared the observed rate of convergence on individual Purkinje cells to chance level, using a bootstrap method based on the relative prevalence of responses to each stimulus (cf. Fig. 5). The difference from chance is indicated by Z values. All combinations occurred more often than expected ($Z > 0$). The P values of these correlations underwent Benjamini–Hochberg correction for multiple comparisons. ** $P < 0.01$.

stimuli. A full correlation analysis on this dataset (Fig. 8A) revealed similar results as the pair-wise comparisons shown in Fig. 6A. A partial correlation analysis found reduced correlations, confirming the existence of a common factor. However, some, but not all, pair-wise combinations occurred above chance level (Fig. 8B). If Purkinje cells respond to a generic sensory event, irrespective of stimulus location, such deviations from

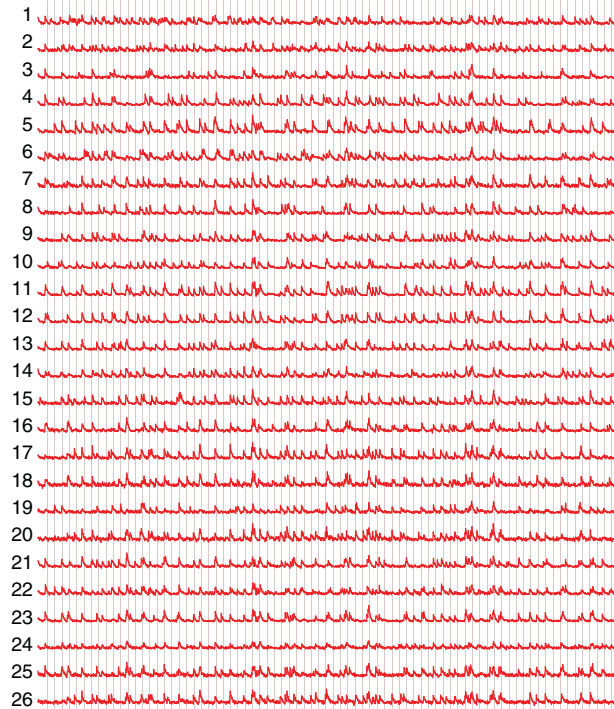
chance are not expected. Therefore, this analysis confirms the idea of a combination of a generic and an input-specific response. The impact of the common factor, representing a generic sensory trigger, was further investigated using principal component analysis performed on the 4×188 matrix containing the Z-scored response peaks from all Purkinje cells receiving all four tactile stimuli. The first component explained 45% of the variance, which is significantly more than expected by chance (32%; Fig. 8C) and confirms that somatosensory input to Purkinje cells is only partially related to the specific stimulus location.

The lower lip and the cheek contributed the most to the first principal component (inset in Fig. 8C). This is in line with them having larger variances (lower lip: 4.72; cheek: 4.86) than the whisker pad (2.89) and the upper lip (3.65). Thus, the lower lip and the cheek were more in line with the generic input than whisker pad and upper lip.

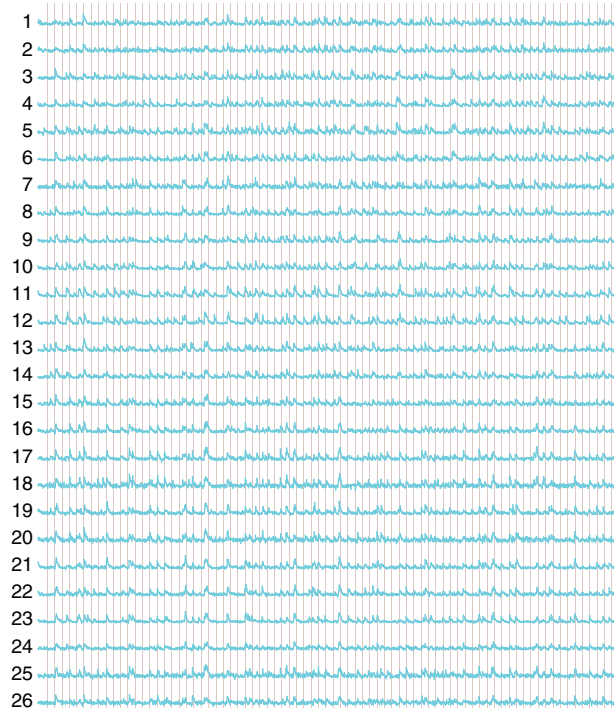
To visualize the relationship between a generic somatosensory response and input specificity, we made a scatter plot between the average peak responses to the four tactile stimuli *versus* the peak responses to each stimulus per Purkinje cell (Fig. 8D). As in Fig. 4B, our data do not support unambiguous discrimination between ‘sensory’ and ‘non-sensory’ Purkinje cells. Several Purkinje cells did not show much of a tactile response to any given stimulus location, while there are also Purkinje cells that showed clear responses. The minimal and maximal responses diverge when the average response is stronger (Fig. 8E). As the average response depends on the minimal and maximal responses, this is not an independent measure. However, when correlating the minimal and maximal responses directly, a similar pattern emerges: stronger minimal responses correlate with even stronger maximal responses (Spearman’s correlation: $r = +0.56$, $P < 0.001$). In other words, Purkinje cells that respond to somatosensory stimulation at any given facial location are also prone to react to stimulation at another spot on the face. However, the Purkinje cells with a stronger ‘generic response’ also had a stronger bias towards one or a few stimulus locations. Again, complex spike responses seem to be involved in the combination and not the segregation of sensory inputs, at the expense of a loss of input specificity. Similar analyses relating to auditory and visual stimulation showed that these conclusions generalize to other sensory modalities (Fig. 8F and G).

and $P < 0.001$. B, we performed a similar analysis focusing only on statistically significant responses (Venn diagrams). Again, all combinations had a positive Z score (as evaluated by a bootstrap method; see Methods), indicating more than expected convergence. The diameter of each circle indicates the fraction of Purkinje cells showing a significant response to that particular, colour-coded stimulus. The size of the bar represents the Z score of the overlapping fraction. C, the same for the combinations of three tactile stimuli. Overall, sensory streams tended to converge, rather than diverge, on Purkinje cells. # $P < 0.10$; * $P < 0.05$, ** $P < 0.01$ and *** $P < 0.001$ (Z test with Benjamini–Hochberg correction).

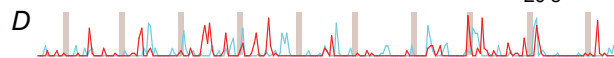
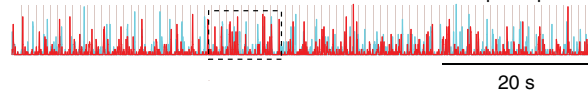
A - Whisker pad stimulation



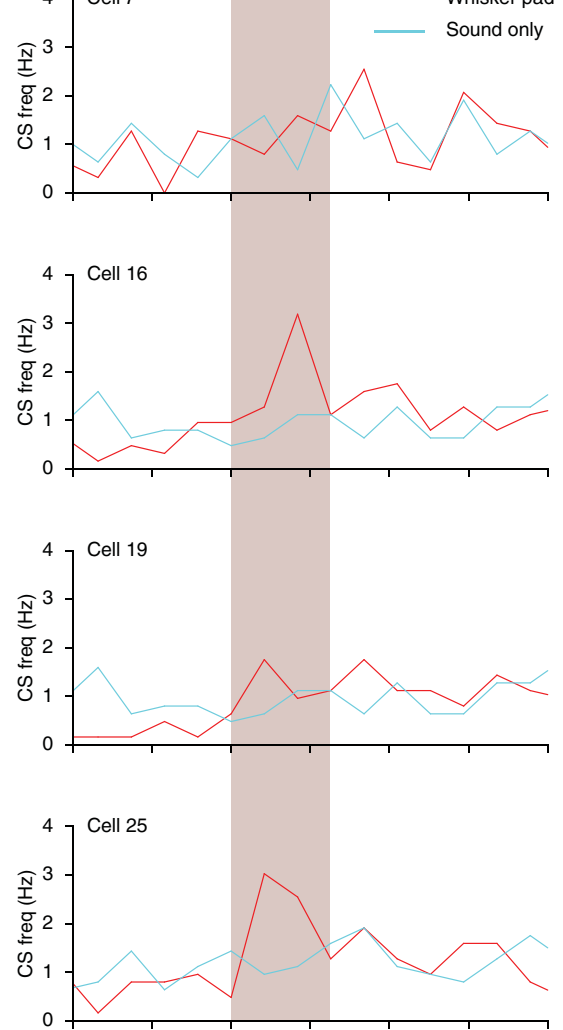
B - Sound only stimulation



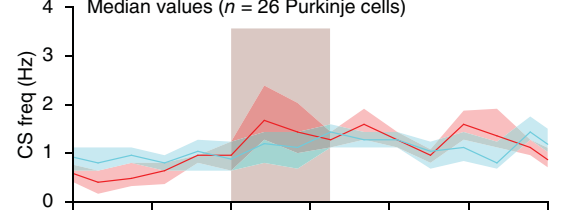
C - Summed complex spikes



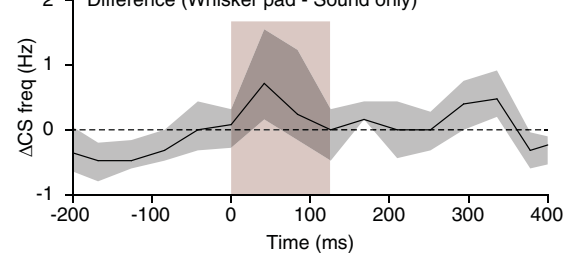
E



F



G



Stimulus strength has limited impact on complex spike responses

To avoid recruiting responses from adjacent areas, we used weak stimulation strengths (Figs 4 and 5). Under anaesthesia, the strength of a stimulus affects the complex spike response probability (Eccles *et al.* 1972; Bosman *et al.* 2010). This finding has been reproduced in awake mice using variations in duration and strength of peri-ocular air puff stimulation (Najafi *et al.* 2014). As a consequence, our approach using weak stimuli could have led to an underestimation of the number and spatial extent of sensory climbing fibre responses. To study whether stimulus strength could also have affected our results, we performed an experiment in which we stimulated all whiskers mechanically with three different strengths, the largest of which was identical to the maximal stimulus we previously applied under anaesthesia (Bosman *et al.* 2010). The chosen stimulus intensities maximized the variation in kinetic energy, which was the most salient feature for barrel cortex neurons (Arabzadeh *et al.* 2004). Stimulus strengths were randomly intermingled (Fig. 9A, B). Raw traces indicate that, even at the ensemble level, weak stimuli do not trigger responses at every trial and spontaneous complex spike firing may occasionally appear as peaks prior to stimulus onset (Figs 2C and 9B, C).

Of the 340 Purkinje cells tested in awake mice, 209 (61%) responded statistically significantly to at least one stimulus strength. In these 209 Purkinje cells, we compared the complex spike responses across three intensities. The weak and the moderate intensities (1 mm displacement reached in 62 ms and 2 mm displacement reached in 31 ms, respectively) showed a comparable number of responses and only the strong stimulus intensity (4 mm reached in 16 ms) evoked significantly more responses ($F_2 = 57.160$, $P < 0.001$, Friedman's test) (Fig. 9D, E). Despite being 16 times faster (250 vs 16 mm/s), the strongest stimulus recruited only 28% (measured as the peak response) or 34% (measured as the integral of the whole response period) more complex spikes than the weakest stimulus (Fig. 9E–G). The same analysis on the whole population of Purkinje cells, including those that did not show a statistically significant response, revealed even less of an impact of stimulus strength, although a small minority of Purkinje cells did show a clear increase in response probability with increased stimulus strength (Fig. 9H).

We therefore conclude that the complex spike response encodes poorly the velocity of whisker displacement in awake mice and that – within boundaries – using stronger stimuli does not necessarily lead to qualitatively different results.

Functionally equivalent Purkinje cells tend to group together

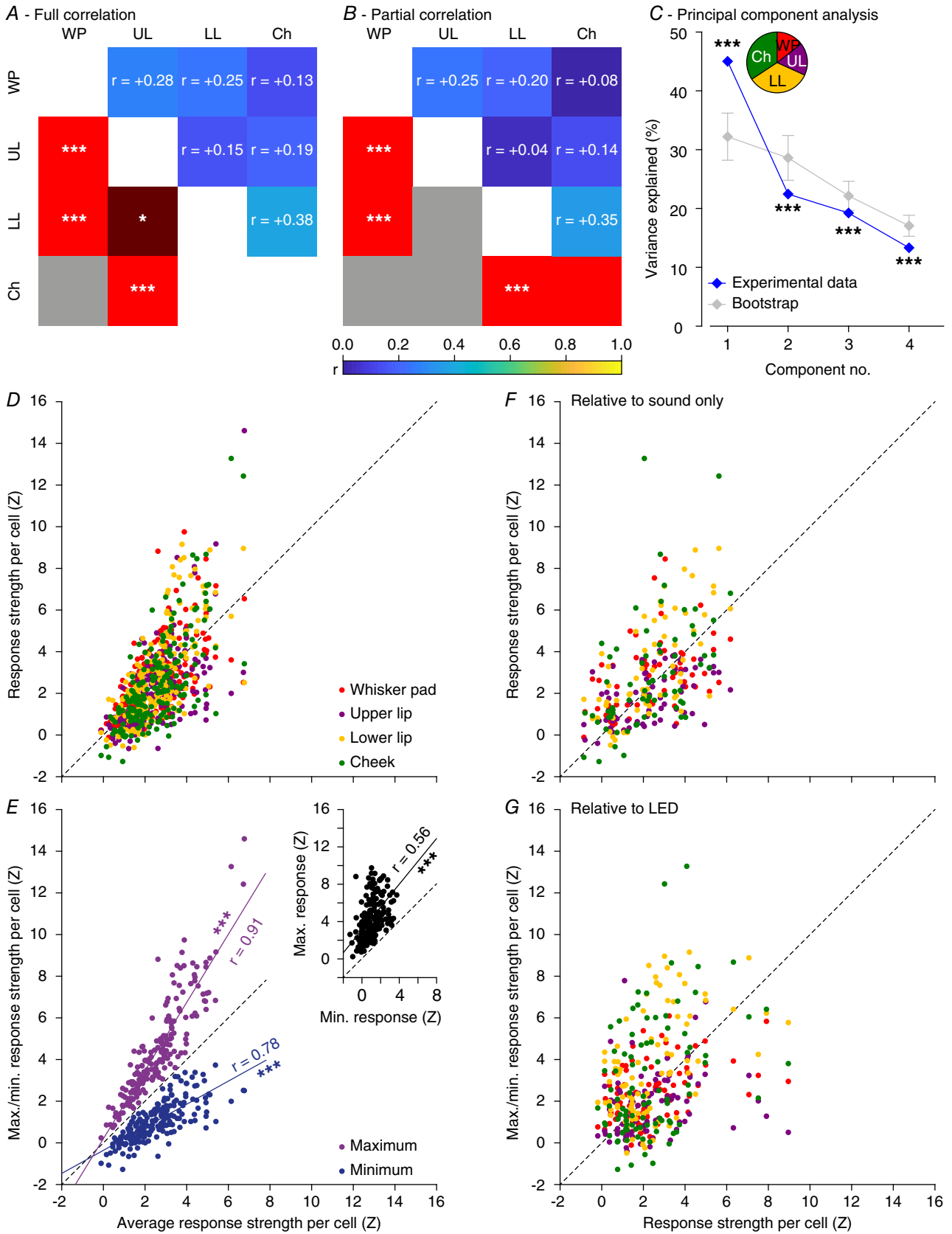
Thus far, we mainly report an abundance of weak and fairly non-specific complex spike responses to mild sensory stimulation. One way in which such weak responses at the cellular level could still have considerable effects at the network level would be when functionally equivalent Purkinje cells would lie together in microzones. Indeed, as the Purkinje cells of each microzone project to a group of adjacent neurons in the cerebellar nuclei (Voogd & Glickstein, 1998; Apps & Hawkes, 2009), population encoding of sensory events may be a form of functional signalling in the olivo-cerebellar system. Figure 10 illustrates to what extent adjacent Purkinje cells have similar stimulus response probabilities. In this example, Purkinje cells responding strongly to whisker pad stimulation are grouped together, but such a spatial clustering does not seem to be perfect, as also a few strongly responsive cells are located in between less responsive Purkinje cells (Fig. 10A) and as upper lip-responsive Purkinje cells are sparsely distributed across the same area (Fig. 10B). We reasoned that spatial clustering should imply that two neighbouring cells have more similar response probabilities than randomly selected cells from the same field of view. This turned out to be the case, but only if we confined our focus to Purkinje cells with statistically significant responses ($Z > 3$) (Fig. 10C, D). Thus, in particular the Purkinje cells with stronger responses to a given stimulus type were located closer together than could be expected from a random distribution.

Single whisker responses in Purkinje cells

Using our tactile stimuli we demonstrated a tendency of nearby Purkinje cells to encode the same stimulus. To study whether this would hold true for even smaller receptive fields we turned to single whisker stimulation.

Figure 7. Sound-only stimulation systematically recruited fewer complex spikes than tactile stimulation

Fluorescence traces of 26 Purkinje cells in a field of view during whisker pad (A) and sound-only (B) stimulation. The moments of stimulation (at 1 Hz) are indicated by the vertical lines. Note that the sound-only stimulation involved the sound of the mechanical device delivering tactile stimuli. Overall, whisker pad stimulation triggered more complex spike responses than sound-only stimulation, as illustrated by the sum of the events (C). The boxed part (10 s) is enlarged in D. E, peri-stimulus time histograms (PSTHs) of four randomly selected Purkinje cells from the experiment illustrated in A and B. In each, the response to whisker pad stimulation was stronger than to sound-only stimulation, which is also reflected in the median of the PSTHs of all 26 Purkinje cells (F) and the median difference between whisker pad and sound-only stimulation (G). The shaded areas indicate the interquartile range.



Using single-unit electrophysiological recordings, we have previously shown that stimulation of a single whisker is sufficient to evoke complex spike responses (Bosman *et al.* 2010). Individual whiskers can be reliably identified across mice and as such they can be qualified as minimal reproducible receptive fields. We repeated our previous single whisker stimulation experiments now using two-photon Ca^{2+} imaging focusing on five whiskers that were stimulated individually in a random sequence. To prevent spontaneous whisking and thereby interference by other whiskers, these experiments were (unlike all other experiments in this study) performed under anaesthesia. In general, the responses were specific, as many Purkinje cells responded to a particular whisker, but not to its neighbouring whiskers (Fig. 11A). Overall, of the 148 Purkinje cells tested, 31 (21%) responded significantly to only one of the five whiskers tested, 14 (10%) to two and five (3%) to three whiskers (Fig. 11B). Not all whiskers were equally effective in recruiting Purkinje cell responses: 23 cells (15%) responded significantly to C3 stimulation, but only four (3%) to C1 stimulation. Likewise, pairs of more anterior whiskers had greater chances of being encoded by the same Purkinje cell (Fig. 11C; Table 5). Thus, also for single whisker stimulation, there was a balance between sensory integration and specificity.

Next, we examined the spatial distribution of responsive Purkinje cells. In Fig. 11D two nearby recording spots from the same mouse are shown. In recording spot 1, from which the example in Fig. 11A originates, all Purkinje cells responded to stimulation of at least one whisker. However, in the second recording spot, only two Purkinje cells responded: both were to a single, but different whisker. For each recording spot we compared responsive *vs.* non-responsive Purkinje cells, taking the average \pm 3 SD of the baseline as the threshold for responsiveness. This yielded a clear separation for the Purkinje cells in the first recording spot, but a rather poor one in the second recording spot (Fig. 11E). In terms of the number

of responsive Purkinje cells and response amplitudes, these two recordings, although made from the same lobule in the same animal, form relatively extreme examples in our dataset. When plotting the response strength *vs.* the fraction of responsive Purkinje cells per field of view, we found a positive correlation (Pearson correlation: $r = +0.52$, $P < 0.001$; Fig. 11F), implying that Purkinje cells with stronger responses to a certain whisker tended to be surrounded by other Purkinje cells encoding the same whisker; this is in line with the much stronger responses in the first than in the second recording spot illustrated in Fig. 11D and E. Together, stimulating single whiskers revealed a similar organization as did the less specific stimuli (see Fig. 10) with a clear tendency of Purkinje cells with the same receptive field to be located close together. However, the spatial clustering was incomplete and weakly responsive Purkinje cells in particular were found to be interspersed with completely unresponsive Purkinje cells.

Functionally equivalent Purkinje cells fire coherently

In addition to spatial clustering, a second requirement for population encoding may be coherence of complex spike firing. While we refer to synchrony of two active Purkinje cells when they fire simultaneously within bins of 2 ms, we define coherence as firing simultaneously within bins of 40 ms. Time frames of 40 ms, which have historically also been described as contemporaneous firing (Wylie *et al.* 1995), fall well within the sub-threshold oscillation cycle of inferior olivary neurons *in vivo* (Khosrovani *et al.* 2007). Under anaesthesia, clusters of Purkinje cells tend to have increased coherence. These clusters organize in parasagittal stripes and their occurrence has been linked to zebrin bands (Sugihara *et al.* 2007; Ozden *et al.* 2009; Tsutsumi *et al.* 2015). To examine whether such parasagittal bands could also be detected in awake mice, we performed a set of imaging experiments with a larger field of view, but at a lower frame rate (15 Hz). Correlation analysis of these data confirmed the

Figure 8. Purkinje cell excitation depends partially, but not completely, on generic sensory input

For the 188 Purkinje cells that received all four tactile stimuli, we calculated the full (A) and partial (B) correlation between the peak responses (in Z scores) of the four different tactile stimuli. This largely confirms the pair-wise correlations illustrated in Fig. 6A. Note, however, that the partial correlations are less pronounced than the full correlations, suggesting the existence of a common component reflecting general excitability, not specific for stimulus location. C, principal component analysis confirmed that a part of the observed variance can indeed be explained by a common factor, as the first principal component of the experimental data is significantly larger than that of bootstrapped data. Error bars indicate the 1–99% confidence interval. The inset shows the relative contributions of the different stimuli to the first principal component. The relatively weak stimuli (lower lip and cheek) were more in tune with the general excitability than the stronger stimuli (whisker pad and upper lip). D, scatter plot showing the correlation between average response strength to the four tactile stimuli *vs.* the four response strengths per Purkinje cell. The Purkinje cells on the left were insensitive to whatever tactile stimulus we presented, while those on the right were sensitive to any tactile stimulus, but showed a bias towards one or a few stimulus locations. This bias becomes more obvious when plotting the minimum and maximum response per Purkinje cell (E). Inset: a strong correlation between the minimum and maximum response strength per Purkinje cell. r values come from Spearman's correlation test. Similar plots were made comparing the sound-only (F) and LED (G) stimulation *vs.* the four tactile stimuli. $*P < 0.05$ and $***P < 0.001$.

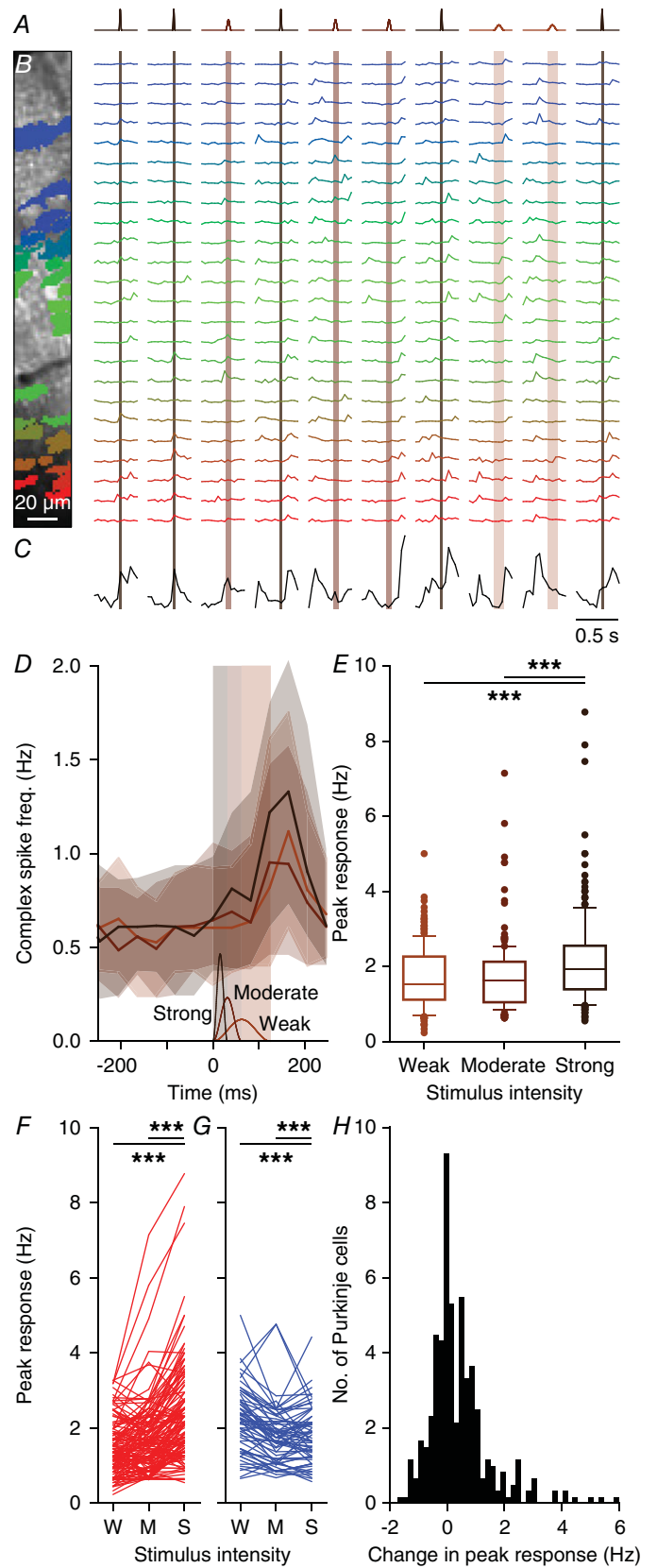


Figure 9. Stimulus strength has only a minor impact on complex spike responsiveness
 A, movements of all large facial whiskers were performed using a piezo-actuator at three different speeds (weak: 1 mm displacement in 62 ms; moderate: 2 mm displacement in 31 ms; strong: 4 mm displacement in 16 ms). The stimulus sequence was randomly permuted. The recordings were made in awake mice. B, field of view with 24 identified and colour-coded Purkinje cells (left) and their corresponding fluorescence traces (right). Stimuli were presented every 2 s and in between trials the laser illumination was briefly blocked to avoid photobleaching. Note that the periods without laser illumination are not drawn to scale. The vertical shaded areas indicate stimulus duration (which was inverse with the stimulus strength). C, summed fluorescence trace composed of all 24 individual traces showing that not all trials evoked ensemble-wide responses. Some spontaneous, inter-trial activity was also observed. D, median number of complex spikes per frame (of 40 ms) per trial (shaded areas: interquartile ranges) for the three stimulus strengths show little difference for the weak and moderate stimulation. The time course and amplitude (1–4 mm) of the three stimuli is shown schematically at the bottom of the graph. Strong stimulation elicited about 30% more complex spikes, as evident from the peak responses for each stimulus intensity. E, box plots showing the response strength for the 209 significantly responsive Purkinje cells (out of 340 Purkinje cells that were measured in this way). F, response rates for all Purkinje cells that showed an increase in response rate with increased stimulus intensity. Only a few cells stand out in that they show a strong response that consistently increases with stimulus strength (lines on top). G, the same for the Purkinje cells that showed a decrease in response strength with increasing stimulus intensity. H, histogram of the differences in peak responses between the strong and the weak stimuli of all 340 recorded Purkinje cells. W = weak; M = moderate; S = Strong; *** $P < 0.001$ (Friedman’s test).

existence of parasagittally oriented clusters, although the demarcation of the clusters was not as sharp as observed under anaesthesia (cf. Ozden *et al.* 2009; Tsutsumi *et al.* 2015) (Fig. 12A–C).

As most of the variation could be found along the medio-lateral axis, we proceeded with smaller fields of views along the medio-lateral axis to allow for a higher temporal resolution. We applied coherence analysis on spontaneous and modulation data obtained from Purkinje cells with significant responses in awake mice. Pairs of Purkinje cells with significant responses upon whisker pad stimulation showed a significantly increased level of coherence ($P < 0.001$;

two-dimensional Kolmogorov–Smirnov test) compared to that of heterogeneous pairs (i.e. pairs of one responsive and one non-responsive Purkinje cell) (Fig. 12D, E). When we examined the firing pattern of the same pairs in the absence of sensory stimulation, we found similar results (Fig. 12F), indicating that it is not the sensory input per se that directs coherence. These findings were confirmed in the whole population, also taking the other tactile and visual stimuli into account (Fig. 12G, H). Only stimulation of the upper lip, the area least represented among the recorded Purkinje cells (Fig. 5B), revealed less discrimination between significantly responsive and heterogeneous pairs. Hence, we conclude that not only spatial clustering but also

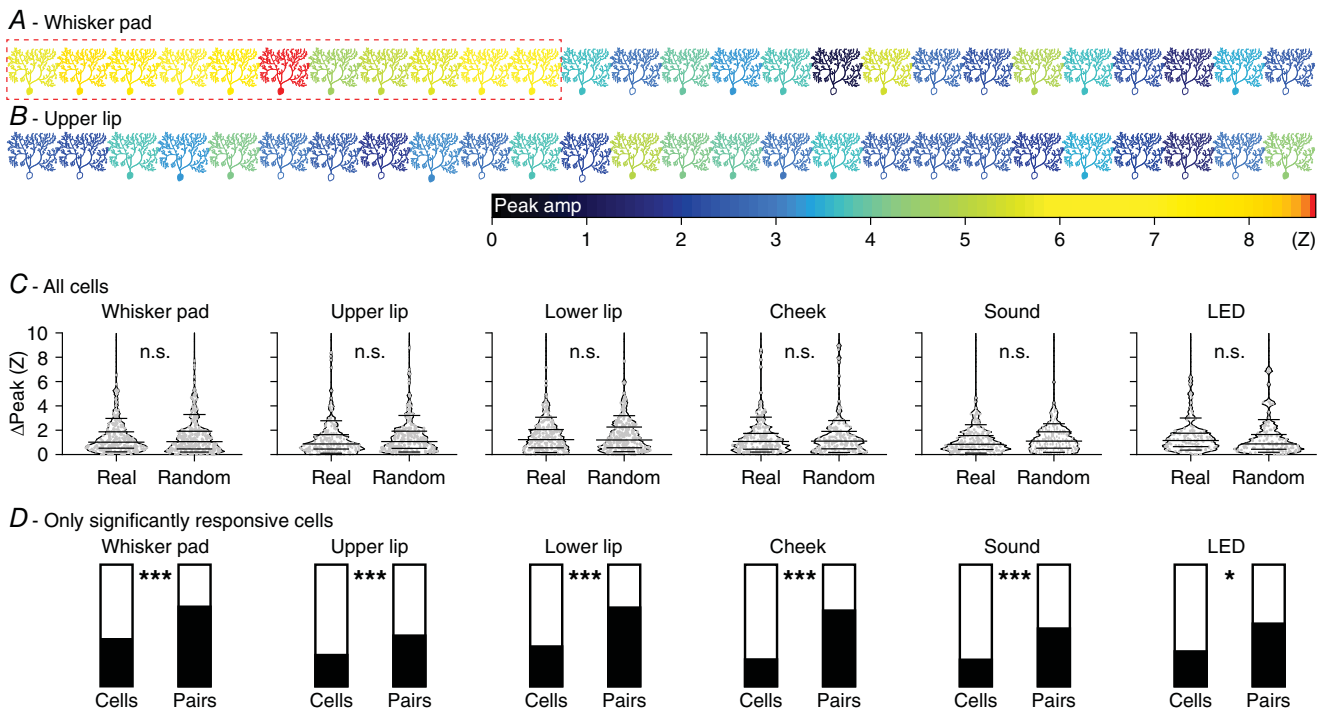


Figure 10. Purkinje cells encoding the same stimulus tend to be spatially grouped

Schematic drawing of a field of view with 26 Purkinje cells organized in the medio-lateral direction of crus 1 in an awake mouse. The colour of each Purkinje cell corresponds to the maximal response to whisker pad (A) or upper lip (B) stimulation. Purkinje cells with a filled soma had a peak response with a Z score > 3 and were considered to be statistically significant, in contrast to those with an open soma. Responsive and non-responsive cells are generally intermingled, but a group of 'strong responders' can be observed for whisker pad stimulation (red rectangle). C, the anecdotal data in A suggest the presence of clusters of Purkinje cells encoding specific stimuli. For this to be the case, one would expect that neighbouring Purkinje cells have roughly similar response strengths. We found that this assumption does not hold as the differences in response strengths of neighbours could not be discriminated from randomly selected cells in the same recording if all Purkinje cells are considered (compared with bootstrap analysis based upon randomly chosen cell pairs within each field of view: all $P > 0.8$; Z test). Data are represented in violin plots, with the grey lines indicating the 10th, 25th, 50th, 75th and 90th percentiles. D, when considering only the Purkinje cells with statistically significant responses, spatial grouping does occur. For each stimulus type, the black portion of the left bar indicates the fraction of Purkinje cells showing a significant response to that stimulus. The filled portion of the right bar indicates the fraction of the neighbours (always on the medial side) of these significantly responsive Purkinje cells that were also significantly responsive. As can be seen, this fraction is always substantially larger than the fraction of significantly responsive Purkinje cells, indicating a tendency of similar Purkinje cells to group together. Statistical significance was tested by comparing the fraction of Purkinje cells with statistically significant responses and the fraction of neighbours of Purkinje cells with statistically significant responses that showed statistically significant responses as well (after correction for border effects) using Fisher's exact test and after Benjamini–Hochberg correction for multiple comparisons: * $P < 0.05$ and *** $P < 0.001$.

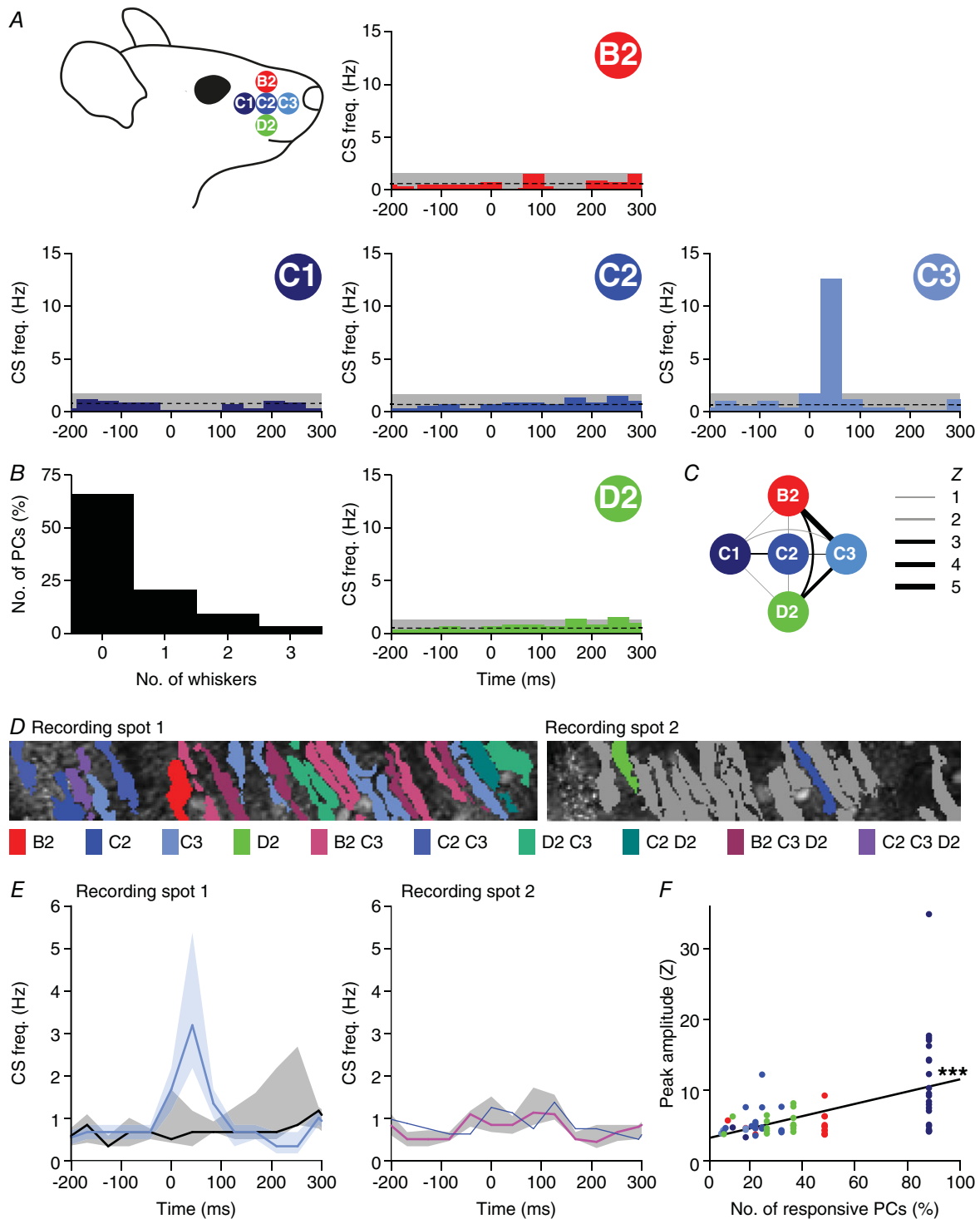


Figure 11. Purkinje cell responses to single whisker stimulation show weak clustering

A, to investigate smaller receptive fields, we sequentially stimulated five of the large facial whiskers. To avoid interference with other whiskers during active movement, we performed these experiments under ketamine/xylazine anaesthesia. Most Purkinje cells, if responsive to single-whisker stimulation, responded only to one of the five whiskers (B). This is illustrated by five peri-stimulus time histograms (PSTHs) from a single, representative Purkinje cell. This particular cell was sensitive to stimulation of the C3 whisker only. The average and 3 SD of the baseline firing are indicated (dashed line and grey area). C, Purkinje cells that responded to more than one whisker were typically responsive to the more anterior whiskers (see also Table 5). The widths of the lines indicate the Z value of the occurrence of multiple responses per cell. D, two recording spots, in close proximity in crus 1

Table 5. Purkinje cell responses to single-whisker stimulation in anaesthetized mice

Whisker	Responsive cells		Difference from chance (Z)			
	No.	%	C1	C2	C3	D2
B2	15 (148)	10	0.630	0.227	5.130***	2.052*
C1	4 (148)	3		0.803	0.782	0.630
C2	17 (148)	11			0.222	0.208
C3	23 (148)	16				3.100**
D2	15 (148)	10				

Purkinje cells respond with complex firing to single-whisker stimulation (cf. Fig. 10). For each whisker, the number and percentage of responsive cells is indicated (in parentheses: total number of cells tested) and the observed rate of convergence on individual Purkinje cells was compared to chance level, using a bootstrap methods based on the relative prevalence of a stimulus. Indicated are the Z values. All combinations occurred more often than expected ($Z > 0$). Statistical significance is indicated after Benjamini–Hochberg correction for multiple comparisons. * $P < 0.05$; ** $P < 0.01$; *** $P < 0.001$.

coherence patterning of functionally equivalent Purkinje cells may facilitate population encoding.

Population responses

In general, the level of coherence among functionally equivalent Purkinje cells was relatively low, with a correlation coefficient seldom exceeding 0.3 (Fig. 12). However, in this analysis we did not discriminate between complex spike firing in response to sensory stimulation and complex spikes occurring spontaneously during inter-trial intervals. Therefore, we subsequently quantified the distribution of complex spikes over time, segregating both types of spikes. This is illustrated for a representative field of view in Fig. 13A. For each frame, we summed all complex spikes of the 17 Purkinje cells in this field of view and subsequently made an aggregate PSTH of all these Purkinje cells, whereby we colour-coded the number of complex spike recorded per frame (see also Romano *et al.* 2018). Frames with only a single event are labelled with a black background and frames with multiple events have a brown background. The darker the shade of brown, the more complex spikes occurred simultaneously. Clearly,

the darker shades – and thus the stronger coherence – were observed during the stimulus response period. This occurrence of coherent firing over time was compared with a random redistribution of the spikes per Purkinje cell (based upon a Poisson distribution). Note that an equal distribution would imply on average fewer than two complex spikes being fired during each frame of 40 ms, indicating the highly patterned distribution found during the experiments. The grey bars in Fig. 13B indicate the level of coherence that could be expected by chance, while the red bars indicate highly unlikely values. This shows that in particular the higher levels of coherence are task-related, while spatially isolated firing occurs irrespective of stimulation.

Examination of the aggregate PSTHs confirms what was already seen in Fig. 4D, in that there is a trend of reduced inter-trial firing for those stimuli with a relatively strong response (Fig. 13A, B). In this experiment, we plotted the responses to air puff stimulation, which recruited statistically significant responses in 17 out of 17 Purkinje cells, on top of those to lower lip stimulation, which recruited only one of the 17 Purkinje cells, illustrating the reduced baseline firing during air puff stimulation (Fig. 13C). When we calculated the average complex spike firing for each stimulus condition over the whole population of recorded Purkinje cells, we found that it was remarkably constant. Even 1 Hz air puff stimulation, able to recruit strong complex spike responses, did not result in increased complex spike firing as compared to an epoch without any form of stimulation (Fig. 13D), pointing towards a homeostatic mechanism within the inferior olive that balances out complex spike firing over longer time intervals.

Homeostasis of complex spike firing

To further study the impact of complex spike homeostasis, we averaged the PSTHs of all Purkinje cells with statistically significant responses to air puff stimulation and compared these to the firing rate in recordings made in the absence of stimulation (using pseudo-triggers generated at the same 1 Hz rate). This pair-wise comparison confirmed that the increase in complex spike firing during the sensory-induced responses comes at the expense of inter-trial firing. The same was true for the milder whisker pad stimulation. However, because the

of the same animal, with the identified Purkinje cell dendritic trees. For each dendrite, the colour indicates the whisker(s) to which it was responsive (see legend below with grey denoting the absence of a statistically significant response). *E*, for each of the two recording sites, the medians of the responsive and the non-responsive Purkinje cells are indicated (to the C3 whisker in the left panel and to the C2 whisker in the right panel). Note that only a single cell was responsive to C2 stimulation in recording spot 2. The shades indicate interquartile ranges. *F*, linear regression revealed that Purkinje cells that were surrounded by other Purkinje cells responsive to the same whisker (same colour code as in *A*) tended to show stronger responses to stimulation of that whisker than Purkinje cells that were more isolated. The *x*-axis represents the fraction of Purkinje cells responsive to the particular whisker within the respective field of view. $r = +0.52$, $P < 0.001$.

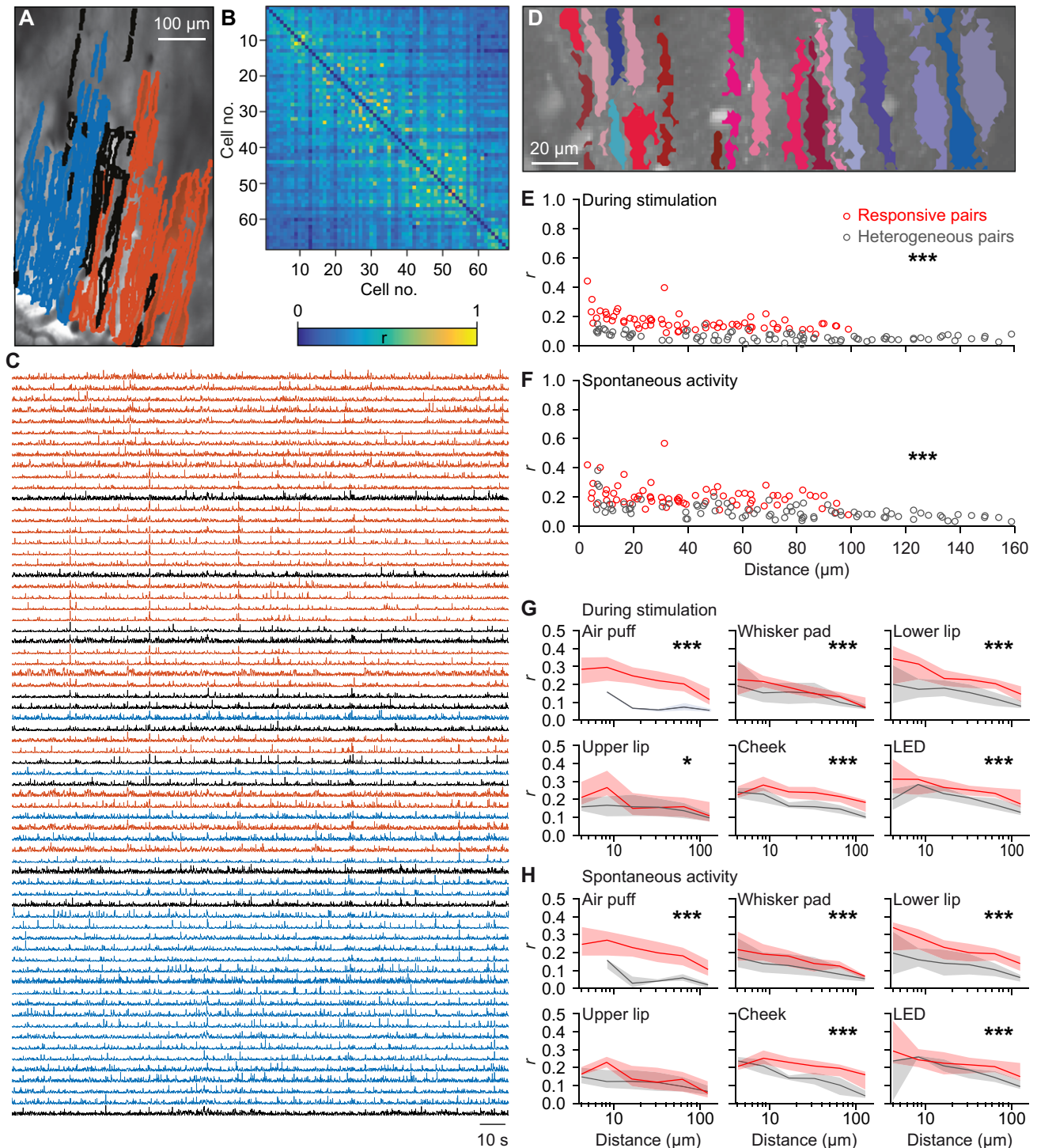


Figure 12. Purkinje cells encoding the same response are closer together

A, to compare the extent of synchronous firing between the medio-lateral and the antero-posterior axes, we made recordings with a larger field of view. Identified Purkinje cell dendrites in a representative field of view colour-coded according to their membership of one of the two clusters identified with meta k means clustering (Dunn index = 0.85). The dendrites indicated in grey could not be contributing to either of the two groups. B, heat map of the pair-wise comparisons of the correlation between the firing of the dendrites shown in A. Although two clusters were identified, it is clear that under our recording conditions, synchronous firing is not strictly related to a single micro-zone. C, raw traces of the neurons indicated in A and B. D, as most of the variation was along the medio-lateral axis, we continued with smaller fields of view oriented along the medio-lateral axis. Representative field of view with segmented PC dendrites. Non-responsive cells are depicted in shades of blue and responsive

responses were weaker, the effect on the inter-trial firing was less than that following strong air puff stimulation. The homeostatic effect was also observed following visual stimulation, although this type of stimulation induced an oscillatory response, making the effect less visible (Fig. 14A, B). Taking the whole population into account, and thus also the Purkinje cells without a statistically significant response, there proved to be a negative correlation between the peak of the stimulus response and the change in inter-trial firing, implying that stronger responses correlated with stronger decreases during the inter-trial period ($r = -0.40$, $P = 0.001$ and $r = -0.31$, $P = 0.001$, Pearson correlations for air puff and whisker pad stimulation, respectively; Fig. 14C). Only following visual stimulation was this correlation less obvious ($r = -0.20$, $P = 0.201$, Pearson correlation after Benjamini–Hochberg correction), possibly due to the oscillatory responses evoked by visual stimulation.

Discussion

Complex spike firing may appear notoriously unpredictable as its spontaneous frequency is low, yet sustained, and its response rate is at best moderate, with large jitters and an ambiguous relationship to stimulus strength. This raises the question as to how the inferior olive relays its signals over time. Possibly, simultaneous complex spike firing by neighbouring Purkinje cells might jointly represent a stimulus, together covering the required signalling for a particular temporal domain (Sasaki *et al.* 1989; Lang *et al.* 1999; Sugihara *et al.* 2007; Ozden *et al.* 2009; Schultz *et al.* 2009). Furthermore, the spatial relationship between somatotopic patches and parasagittally oriented microzones has not been clarified in terms of complex spike signalling, and it is not understood to what extent this relationship also depends on the temporal context in which the signals are generated.

Here, we investigated at the level of individual Purkinje cells whether encoding of somatosensory input from different facial areas in lobule crus 1 occurs in striped microzones or instead follows a more fractured arrangement. Mild touches at localized facial areas revealed a loose version of fractured somatotopy. Purkinje

cells with the same receptive field tended to be located in each other's neighbourhood, but the spatial organization was not very strict, as highly responsive Purkinje cells were sometimes observed amidst non-responsive ones. Functionally equivalent, adjacent Purkinje cells showed increased coherence in their complex spike firing, in particular in response to sensory stimulation. Moreover, homeostatic mechanisms were engaged, ensuring that over longer periods complex spike firing rates are constant, making the short-lived coherent responses more salient.

The functional role of climbing fibre activity

Clinical manifestations of inferior olivary dysfunction range from ataxia and tremor to autism spectrum disorders (Llinás *et al.* 1975; Samuel *et al.* 2004; Bauman & Kemper, 2005; Welsh *et al.* 2005; Lim & Lim, 2009; De Gruijl *et al.* 2013). Climbing fibre-evoked complex spikes are also essential for the proper timing, size and direction of movements as well as for the encoding of expected and unexpected deviations from planned movements (Wang *et al.* 1987; Simpson *et al.* 1996; Kitazawa *et al.* 1998; Ito, 2013; Yang & Lisberger, 2014; Herzfeld *et al.* 2018; Romano *et al.* 2018). In addition, climbing fibre activity is crucial for cerebellar learning by controlling synaptic plasticity at a wide variety of synapses in the molecular layer of the cerebellar cortex (Ito & Kano, 1982; Ito, 2003; Coesmans *et al.* 2004; Van Der Giessen *et al.* 2008; Gao *et al.* 2012). Despite these many functions, complex spike firing is remarkably stable over longer intervals, suggesting that the impact of complex spikes is strongly context-dependent.

This context is provided by the synaptic inputs to the inferior olive that relay information from excitatory ascending and descending pathways as well as inhibitory projections from the hindbrain (De Zeeuw *et al.* 1998). Both types converge on each individual spine present on the dendrites of the inferior olivary neurons (De Zeeuw *et al.* 1989, 1990). The inhibitory input predominantly originates from the cerebellar nuclei, implying that part of the context is mediated by one of the target regions of the climbing fibres themselves. This feedback is engaged in a closed loop, as individual climbing fibres of each olivary subnucleus project to the Purkinje cells located within a specific parasagittal zone (Sugihara *et al.* 2001)

cells in shades of red during whisker pad stimulation. *E*, for each pair of Purkinje cells we calculated the correlation coefficient (r) during 1 Hz whisker pad stimulation. The pairs of two Purkinje cells that were both responsive to whisker pad stimulation had on average a higher level of synchrony than the pairs connecting a responsive and a non-responsive Purkinje cell ($P < 0.001$; two-dimensional Kolmogorov–Smirnov test). The pairs consisting of two non-responsive Purkinje cells were excluded from this analysis. *F*, interestingly, even in the absence of sensory stimulation, the pairs of Purkinje cells that were both responsive to whisker pad stimulation maintained a higher level of synchrony than 'heterogeneous pairs'. Thus, Purkinje cells with the same receptive field tended to fire more synchronously, even in the absence of stimulation. This analysis was expanded in the presence (*G*) and absence (*H*) of sensory stimulation for six different types of stimulation and illustrated as the median r value per distance category (six bin values of equal distance at a log scale). The shaded areas represent the interquartile ranges. * $P < 0.05$ and *** $P < 0.001$ (Kolmogorov–Smirnov tests).

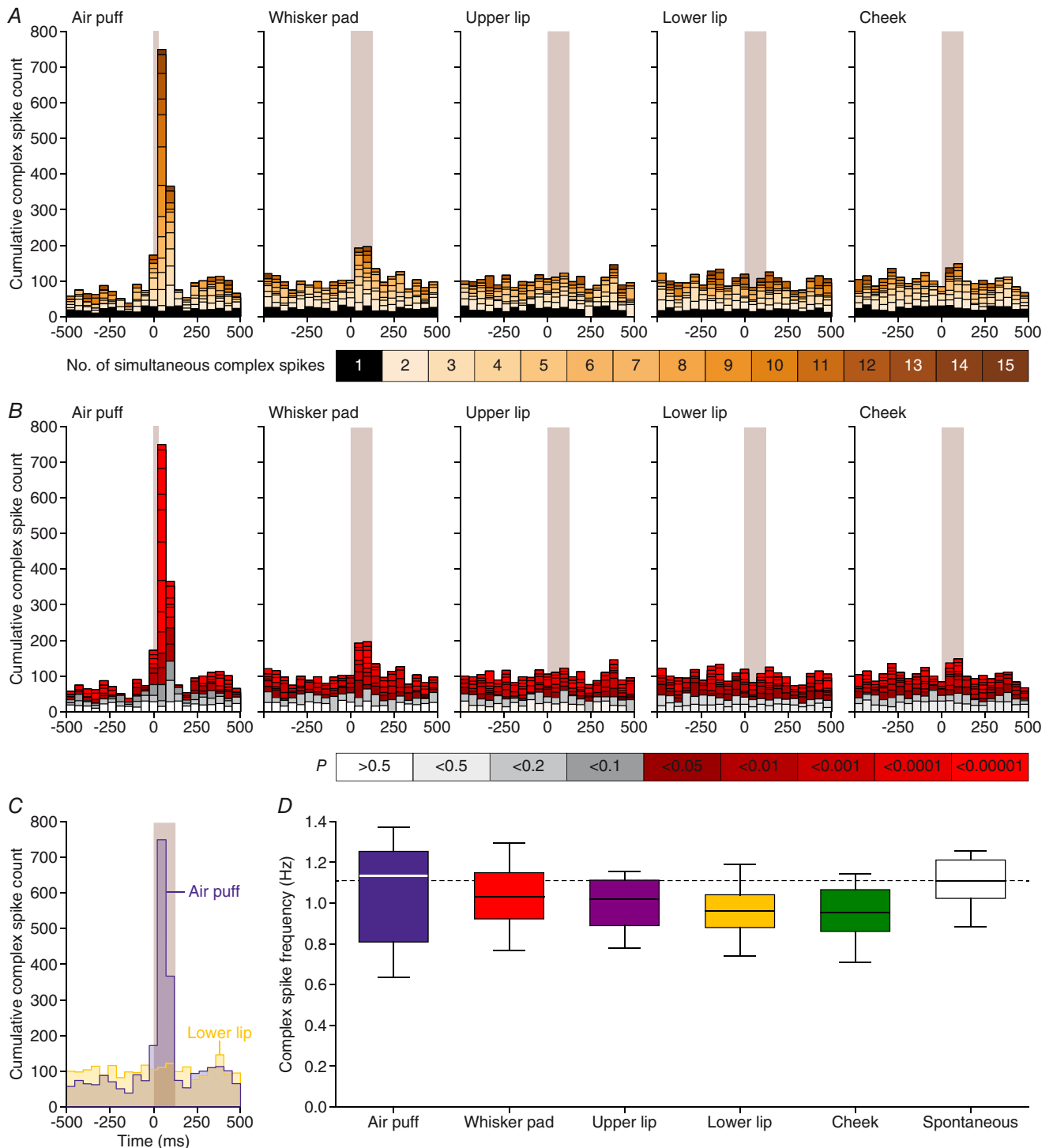


Figure 13. Purkinje cells encode strong and weak sensory stimulation via synchronous firing
 A, aggregate peri-stimulus time histograms (PSTHs) show that coherent firing of complex spikes predominantly occurs following sensory stimulation. For each field of view, we calculated the number of complex spikes occurring per frame, summing those of all Purkinje cells in that field of view. Subsequently, we made aggregate PSTHs where the colour of each bin refers to the number of dendrites simultaneously active. The black fields indicate frames in which only a single dendrite was active. In this field of view, 17 Purkinje cells were measured. Of these, 17 (100%) reacted to air puff, 12 (71%) to whisker pad, 3 (18%) to upper lip, 4 (24%) to lower lip and 1 (6%) to cheek stimulation. B, based on a Poisson distribution of complex spikes over all dendrites and bins, one would expect between 0 and 3 simultaneously active dendrites (grey bars). The red bars indicate events involving more dendrites simultaneously than expected from a random distribution. Thus, the sparse firing as expected by chance

that converge on the neurons in the cerebellar nuclei that project back to the same olivary subnucleus where the loop started (Groenewegen *et al.* 1979; Voogd & Glickstein, 1998; Apps *et al.* 2018). Each module can be further subdivided into microzones within which complex spike coherence is clearly enhanced upon strong stimulation (Ozden *et al.* 2009; Tsutsumi *et al.* 2015), a phenomenon that is promoted by strong electrotonic coupling within olivary glomeruli (Sotelo *et al.* 1974; Ruigrok *et al.* 1990; Devor & Yarom, 2002; De Gruijl *et al.* 2014). Under anaesthesia, complex spike coherence adheres relatively well to the delineation of zebrin bands (Sugihara *et al.* 2007; Ozden *et al.* 2009; Tsutsumi *et al.* 2015). In awake mice, the spatial and functional demarcation between adjacent coherent clusters of Purkinje cells is diminished (Fig. 12B; De Gruijl *et al.* 2014), probably due to the more diverse pattern of synaptic input to the inferior olive present in awake mice. Thus, although anatomical and functional data support the microzonal organization, the activity patterns are best understood as produced dynamically depending on the behavioural context that is transmitted via cerebellar and extra-cerebellar synaptic input (Negrello *et al.* 2019).

A particularly interesting model system to study differential functional roles of climbing fibre activity is classical eyeblink conditioning. Subjects can readily learn to associate a previously neutral stimulus with an aversive puff to the eye. Before training, complex spikes virtually only occur after the unconditioned air puff stimulus. However, after training, the initially neutral stimulus, the conditioned stimulus, also reliably triggers complex spike responses at the onset time of the conditioned response (Halverson *et al.* 2015; Ohmae & Medina, 2015; Ten Brinke *et al.* 2015). It appears that the nature of the conditioned stimulus, whether auditory, visual or tactile (Hilgard & Marquis, 1936; McCormick & Thompson, 1984; Das *et al.* 2001; Galvez *et al.* 2006), is of subordinate relevance in this respect and that the main goal of these conditioned stimulus-related complex spikes is to further improve the conditioned motor response (Ohmae & Medina, 2015; Ten Brinke *et al.* 2015, 2019). However, the conditioned stimulus does not generalize: subjects trained with a visual conditioned stimulus will not blink after receiving an auditory stimulus for instance, although the associative learning process for a second stimulus goes faster than for the first (Kehoe & Holt, 1984; Campolattaro & Freeman, 2009; Campolattaro *et al.* 2015). Such a flexible

arrangement would be very much in line with our data. In a naïve mouse, multiple weak sensory streams as well as internally generated sensorimotor prediction signals may converge on individual Purkinje cells (present study; Heffley *et al.* 2018). Consequently, most sensory stimuli trigger only weak complex spike responses. Given the behavioural saliency, one or a few pathways may grow stronger and account for the Purkinje cells with a strong complex spike response. Thus, there is a balance between generalized input, encoding basically any sensory or internally generated event, and input-specificity.

To what extent motor-related enhancement of complex spikes responses as observed during eyeblink conditioning are module-dependent remains to be shown. In principle such responses might be dominant in zebrin-negative modules, in which simple spike responses are suppressed during learning (De Zeeuw & Ten Brinke, 2015) and in which climbing fibre responses can further facilitate such suppression (Ten Brinke *et al.* 2015). In zebrin-positive zones, in which the expression of learned responses are more driven by increases of simple spike responses (De Zeeuw & Ten Brinke, 2015; Voges *et al.* 2017; Romano *et al.* 2018), the opposite might occur. For example, it has been shown that olivary activity can be inhibited and gated when sensory stimuli are applied in a predictable fashion during self-generated locomotion (Gibson *et al.* 2004).

Receptive fields of Purkinje cells and population coding

Several existing maps of somatosensory representations of complex spike activity suggest a fractured somatotopy (Miles & Wiesendanger, 1975; Rushmer *et al.* 1980; Castelfranco *et al.* 1994). These maps were typically created by establishing, for each recording position, the strongest input region, disregarding information on convergence of multiple inputs. However, these studies made clear that climbing fibres could have receptive fields of widely different sizes, expanding to structures as large as a whole limb (Thach, 1967; Leicht *et al.* 1973). The predominant somatosensory input to crus 1 stems, according to the classification of mossy fibre inputs, from the facial whiskers (Shambes *et al.* 1978). Here, we show at single cell resolution that climbing fibres indeed do convey somatosensory input from different facial areas, with Purkinje cells having the same receptive fields being located preferably in each other's proximity.

is relatively constant throughout the trials, but the simultaneous activity of multiple dendrites is strongly enhanced following sensory stimulation. *C*, direct overlay of the aggregate PSTHs in response to air puff and lower lip stimulation showing that the strong response found after air puff stimulation comes at the expense of intertrial complex spikes (152 trials per condition). *D*, for equally long recordings in the presence of different types of stimulation, equal complex spike frequencies were observed as during spontaneous activity ($F_{2,544,20,348} = 2.561$, $P = 0.091$, repeated-measures ANOVA), indicating that sensory stimulation results in a temporal re-ordering of complex spikes, rather than to the production of more complex spikes.

Our data reveal that classification of Purkinje cells into responsive and non-responsive cells is at best disputable, with the large majority of Purkinje cells typically showing relatively weak responses (Fig. 4B). Whisker pad stimulation elicits the strongest responses

in lateral crus 1 (Romano *et al.* 2018), while most of the current data were collected in more medial parts of crus 1. Consequently, only a few Purkinje cells included in the present study showed a strong response to whisker stimulation. Remarkably, these were the ones that did

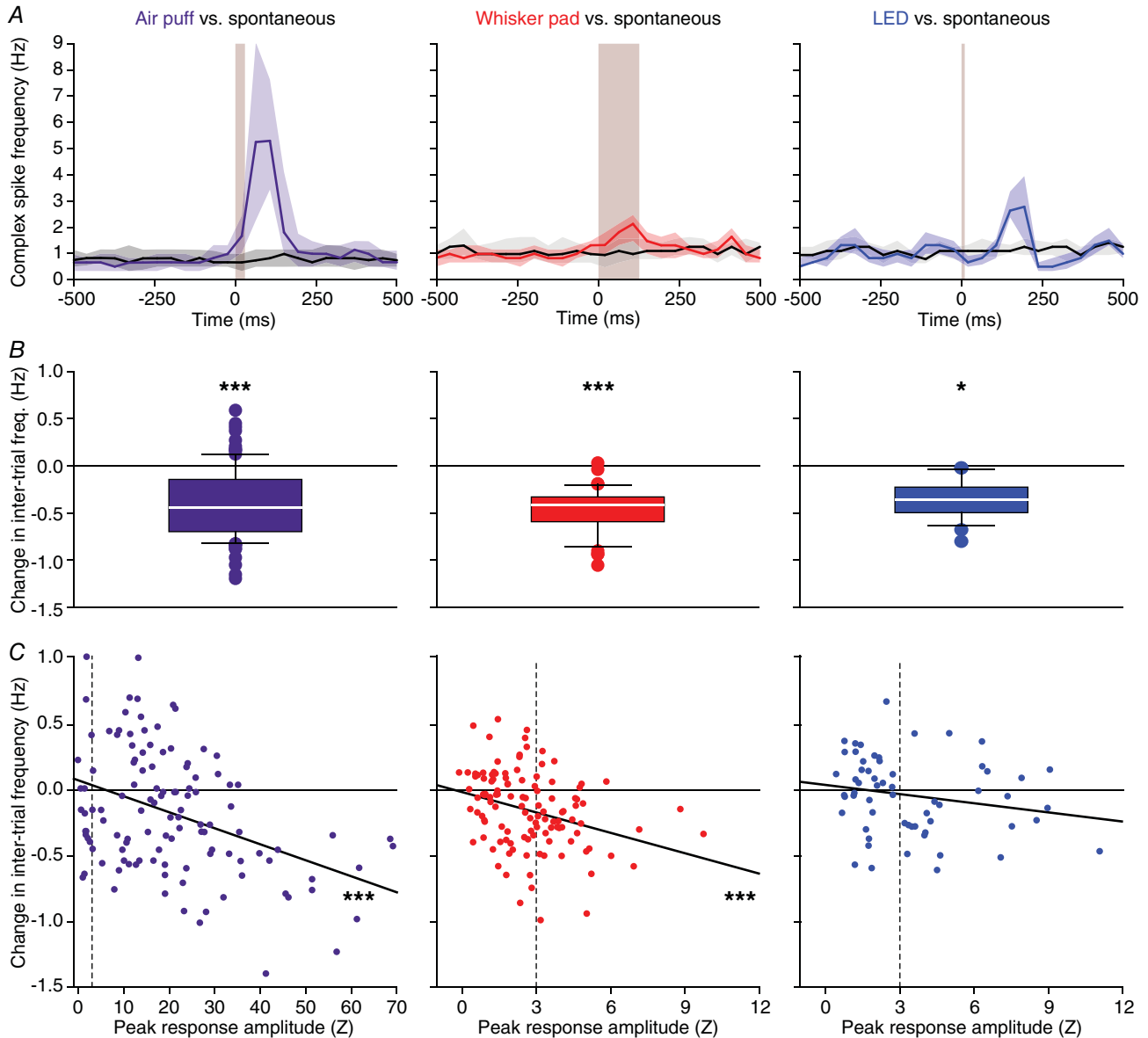


Figure 14. Sensory stimulation results in a temporal re-ordering of complex spikes

A, the temporal distribution of complex spikes was compared in a pair-wise fashion between sessions with sensory stimulation and sessions without. For this analysis, we included only Purkinje cells that displayed a statistically significant response to the stimulus involved ($n = 102$ for air puff, $n = 45$ for whisker pad and $n = 27$ for visual stimulation). The spontaneous recordings were analysed by creating *post hoc* pseudo-stimuli at the same 1 Hz frequency as during sensory stimulation. Shown are the medians of the peri-stimulus time histograms. The shaded areas indicate the interquartile ranges. B, the reduction in baseline firing, measured during the interval -500 to -250 ms, was significant in all cases (Wilcoxon matched-pairs test after Benjamini–Hochberg correction for multiple comparisons). C, the larger the response amplitude, the stronger the reduction in inter-trial firing (Pearson correlation tests after Benjamini–Hochberg correction for multiple comparisons). This analysis was performed on all Purkinje cells ($n = 117$ for air puff and whisker pad stimulation and $n = 60$ for LED stimulation; dotted lines mark the criterion for statistical significance at $Z = 3$). Note the differences in the x-axis scaling with the air puff evoking relatively stronger responses. * $P < 0.05$; *** $P \leq 0.001$.

depend on stimulus strength, in contrast to the majority of the weakly responsive Purkinje cells (Fig. 9F, G). This may point to the existence of two groups of Purkinje cells: some that show complex spike responses that clearly depend on stimulus strength, in line with previous reports (Eccles *et al.* 1972; Bosman *et al.* 2010; Najafi *et al.* 2014), and others that display only a weak to moderate sensitivity to a specific sensory input, independent of stimulus strength.

For the Purkinje cells with strong responses, a function in the timing and/or fine-tuning of motor responses is likely. Complex spikes have been shown to adjust saccadic eye movements on a trial-by-trial basis (Yang & Lisberger, 2014; Herzfeld *et al.* 2018). They are also correlated to the amplitude of reflexive whisker movements (Romano *et al.* 2018). The abundance of weak responses could, as discussed above for zebrin-negative modules, possibly be explained in terms of forming a substrate for cerebellar learning, where specific training would strengthen particular pathways as, for instance, occurs during classical eyeblink conditioning (Ten Brinke *et al.* 2015).

An alternative, but not mutually exclusive, explanation for the presence of weak responses could be multi-sensory integration. Analysing the response rates of Purkinje cell ensembles revealed that the density of responsive cells is crucial for shaping the population response. We propose that the weak spatial clustering of Purkinje cells encoding the same stimulus, being interspersed with Purkinje cells receiving input from other sources, and the tendency of coherent firing of Purkinje cells encoding the same stimulus both contribute to the creation of a heterogeneous map of Purkinje cells, where each area encodes a particular functional set of inputs. Each of the properties of the complex spikes seems rather insignificant in isolation, but in combination may result in specific and robust population encoding.

Non-tactile inputs

Light or sound can act as conditional stimulus to recruit increasingly more climbing fibre activity during learning, highlighting the flexibility of this pathway (Ohmae & Medina, 2015; Ten Brinke *et al.* 2015). In naïve animals, auditory and visual input have been shown to project predominantly to the vermis (Snider & Stowell, 1944), but we demonstrate here that visual and auditory input can converge on the same Purkinje cells that encode somatosensory input in crus 1 – also in naïve mice – further strengthening the idea that climbing fibre activity can act as an integrator of contextual input. With visual stimulation the latency was significantly longer than expected. The presented visual stimulus is probably not directly relayed from the retina, but a descending input from the visual cortex or other higher brain regions such as the mesodiencephalic junction (De Zeeuw *et al.* 1998).

Homeostasis of complex spike frequency

The overall firing rate of complex spikes was stable across conditions, with response peaks being compensated for by reduced inter-trial firing (see also Negrello *et al.* 2019). The stronger the response peak, the less inter-trial firing, leading to homeostasis of complex spike firing over longer time periods. Intriguingly, the complex spikes during the inter-trial intervals were predominantly fired by a few, dispersed Purkinje cells and the response peak was largely due to increased coherence. It therefore seems that Purkinje cells display a basic complex spike firing rate, which in the absence of functional behaviour is not coherent with adjacent Purkinje cells. In view of the strong impact of complex spikes on synaptic plasticity (Ito & Kano, 1982; Ito, 2003; Coesmans *et al.* 2004; Gao *et al.* 2012), this could subserve homeostatic functions. Salient stimuli are largely encoded by coherent firing, making them different from non-stimulus-related activity.

Short-lived excursions from the stereotypic 1 Hz complex spike frequency occur often. Many studies have documented a 10 Hz rhythm in complex spike firing (Bell & Kawasaki, 1972; Wylie *et al.* 1995; Lang *et al.* 1999; Blenkinsop & Lang, 2006), which is sustained over longer periods after harmaline application (Llinás & Volkind, 1973). Our current data (e.g. see double spike in Fig. 1D) also show that the inferior olive as well as the Purkinje cells are physically able to fire much faster than at 1 Hz. Several mechanisms may contribute to the homeostatic control of inferior olivary spiking, including the previously mentioned olivo-cerebellar loops. Disrupted Purkinje cell activity can affect climbing fibre activity (Chen *et al.* 2010), and reduced inferior olivary activity leads to enhanced simple spike activity (Montarolo *et al.* 1982), which in turn dampens activity in the GABAergic neurons of the cerebellar nuclei that control the inferior olive (Chaumont *et al.* 2013; Witter *et al.* 2013). The interplay between glutamatergic input to the neurons of the inferior olive, intracellular signalling and electrotonic coupling may also lead to homeostatic control of complex spike firing via protein kinase A (PKA) and β Ca²⁺/calmodulin-dependent protein kinase II (β CaMKII) (Mathy *et al.* 2014; Bazzigaluppi *et al.* 2017). Overall, the inferior olive functions at the crossroads of well-defined and rigid anatomical structures and highly dynamic synaptic input, while subject to homeostatic control, the sources of which remain partly to be determined.

References

- Albus JS (1971). Theory of cerebellar function. *Math Biosci* **10**, 25–61.
- Andersen P, Eccles JC & Voorhoeve PE (1964). Postsynaptic inhibition of cerebellar Purkinje cells. *J Neurophysiol* **27**, 1138–1153.

- Apps R & Garwicz M (2005). Anatomical and physiological foundations of cerebellar information processing. *Nat Rev Neurosci* **6**, 297–311.
- Apps R & Hawkes R (2009). Cerebellar cortical organization: a one-map hypothesis. *Nat Rev Neurosci* **10**, 670–681.
- Apps R, Hawkes R, Aoki S, Bengtsson F, Brown AM, Chen G, Ebner TJ, Isope P, Jorntell H, Lackey EP, Lawrenson C, Lumb B, Schonewille M, Sillitoe RV, Spaeth L, Sugihara I, Valera A, Voogd J, Wylie DR & Ruigrok TJH (2018). Cerebellar modules and their role as operational cerebellar processing units. *Cerebellum* **17**, 654–682.
- Arabzadeh E, Panzeri S & Diamond ME (2004). Whisker vibration information carried by rat barrel cortex neurons. *J Neurosci* **24**, 6011–6020.
- Axelrad H & Crepel F (1977). Représentation sélective des vibrisses mystaciales au niveau des cellules de Purkinje du cervelet par la voie des fibres grimpantes chez le rat. *C R Acad Sci Hebd Seances Acad Sci D* **284**, 1321–1324.
- Bauman ML & Kemper TL (2005). Neuroanatomic observations of the brain in autism: a review and future directions. *Int J Dev Neurosci* **23**, 183–187.
- Bazzigaluppi P, Isenia SC, Haasdijk ED, Elgersma Y, De Zeeuw CI, van der Giessen RS & de Jeu MTG (2017). Modulation of murine olivary connexin 36 gap junctions by PKA and CaMKII. *Front Cell Neurosci* **11**, 397.
- Bell CC & Kawasaki T (1972). Relations among climbing fiber responses of nearby Purkinje cells. *J Neurophysiol* **35**, 155–169.
- Blenkinsop TA & Lang EJ (2006). Block of inferior olive gap junctional coupling decreases Purkinje cell complex spike synchrony and rhythmicity. *J Neurosci* **26**, 1739–1748.
- Bloedel JR & Ebner TJ (1984). Rhythmic discharge of climbing fibre afferents in response to natural peripheral stimuli in the cat. *J Physiol* **352**, 129–146.
- Bosman LWJ, Houweling AR, Owens CB, Tanke N, Shevchouk OT, Rahmati N, Teunissen WHT, Ju C, Gong W, Koekkoek SKE & De Zeeuw CI (2011). Anatomical pathways involved in generating and sensing rhythmic whisker movements. *Front Integr Neurosci* **5**, 53.
- Bosman LWJ, Koekkoek SKE, Shapiro J, Rijken BFM, Zandstra F, van der Ende B, Owens CB, Potters JW, de Gruijl JR, Ruigrok TJH & De Zeeuw CI (2010). Encoding of whisker input by cerebellar Purkinje cells. *J Physiol* **588**, 3757–3783.
- Brown IE & Bower JM (2002). The influence of somatosensory cortex on climbing fiber responses in the lateral hemispheres of the rat cerebellum after peripheral tactile stimulation. *J Neurosci* **22**, 6819–6829.
- Campolattaro MM, Buss EW & Freeman JH (2015). Cross-modal savings in the contralateral eyelid conditioned response. *Behav Neurosci* **129**, 683–691.
- Campolattaro MM & Freeman JH (2009). Cerebellar inactivation impairs cross modal savings of eyeblink conditioning. *Behav Neurosci* **123**, 292–302.
- Castelfranco AM, Robertson LT & McCollum G (1994). Detail, proportion, and foci among face receptive fields of climbing fiber responses in the cat cerebellum. *Somatosens Mot Res* **11**, 27–46.
- Cominari NL, Lang EJ, Sillitoe RV & Apps R (2015). Redefining the cerebellar cortex as an assembly of non-uniform Purkinje cell microcircuits. *Nat Rev Neurosci* **16**, 79–93.
- Chaplan SR, Bach FW, Pogrel JW, Chung JM & Yaksh TL (1994). Quantitative assessment of tactile allodynia in the rat paw. *J Neurosci Methods* **53**, 55–63.
- Chaumont J, Guyon N, Valera AM, Dugué GP, Popa D, Marcaggi P, Gautheron V, Reibel-Foisset S, Dieudonné S, Stephan A, Barrot M, Cassel JC, Dupont JL, Doussau F, Poulain B, Selimi F, Léna C & Isope P (2013). Clusters of cerebellar Purkinje cells control their afferent climbing fiber discharge. *Proc Natl Acad Sci U S A* **110**, 16223–16228.
- Chen X, Kovalchuk Y, Adelsberger H, Henning HA, Sausbier M, Wietzorrek G, Ruth P, Yarom Y & Konnerth A (2010). Disruption of the olivo-cerebellar circuit by Purkinje neuron-specific ablation of BK channels. *Proc Natl Acad Sci U S A* **107**, 12323–12328.
- Coemans M, Weber JT, De Zeeuw CI & Hansel C (2004). Bidirectional parallel fiber plasticity in the cerebellum under climbing fiber control. *Neuron* **44**, 691–700.
- Das S, Weiss C & Disterhoft JF (2001). Eyeblink conditioning in the rabbit (*Oryctolagus cuniculus*) with stimulation of the mystacial vibrissae as a conditioned stimulus. *Behav Neurosci* **115**, 731–736.
- De Gruijl JR, Bosman LWJ, De Zeeuw CI & De Jeu MTG (2013). Inferior olive: all ins and outs. In *Handbook of the Cerebellum and Cerebellar Disorders*, ed. Manto M, Schmahmann JD, Rossi F, Gruol DL & Koibuchi N, pp. 1013–1058. Springer, Dordrecht.
- De Gruijl JR, Hoogland TM & De Zeeuw CI (2014). Behavioral correlates of complex spike synchrony in cerebellar microzones. *J Neurosci* **34**, 8937–8944.
- De Zeeuw CI, Hoebeek FE, Bosman LWJ, Schonewille M, Witter L & Koekkoek SK (2011). Spatiotemporal firing patterns in the cerebellum. *Nat Rev Neurosci* **12**, 327–344.
- De Zeeuw CI, Holstege JC, Ruigrok TJ & Voogd J (1989). Ultrastructural study of the GABAergic, cerebellar, and mesodiencephalic innervation of the cat medial accessory olive: anterograde tracing combined with immunocytochemistry. *J Comp Neurol* **284**, 12–35.
- De Zeeuw CI, Holstege JC, Ruigrok TJH & Voogd J (1990). Mesodiencephalic and cerebellar terminals terminate upon the same dendritic spines in the glomeruli of the cat and rat inferior olive: an ultrastructural study using a combination of [³H]leucine and wheat germ agglutinin coupled horseradish peroxidase anterograde tracing. *Neuroscience* **34**, 645–655.
- De Zeeuw CI, Simpson JI, Hoogenraad CC, Galjart N, Koekkoek SKE & Ruigrok TJH (1998). Microcircuitry and function of the inferior olive. *Trends Neurosci* **21**, 391–400.
- De Zeeuw CI & Ten Brinke MM (2015). Motor learning and the cerebellum. *Cold Spring Harb Perspect Biol* **7**, a021683.
- Devor A & Yarom Y (2002). Electrotonic coupling in the inferior olivary nucleus revealed by simultaneous double patch recordings. *J Neurophysiol* **87**, 3048–3058.
- Eccles JC, Sabah NH, Schmidt RF & Táboriková H (1972). Cutaneous mechanoreceptors influencing impulse discharges in cerebellar cortex. III. In Purkinje cells by climbing fiber input. *Exp Brain Res* **15**, 484–497.

- Ekerot CF, Garwicz M & Schouenborg J (1991). Topography and nociceptive receptive fields of climbing fibres projecting to the cerebellar anterior lobe in the cat. *J Physiol* **441**, 257–274.
- Galvez R, Weiss C, Weible AP & Disterhoft JF (2006). Vibrissa-signaled eyeblink conditioning induces somatosensory cortical plasticity. *J Neurosci* **26**, 6062–6068.
- Gao W, Chen G, Reinert KC & Ebner TJ (2006). Cerebellar cortical molecular layer inhibition is organized in parasagittal zones. *J Neurosci* **26**, 8377–8387.
- Gao Z, Van Beugen BJ & De Zeeuw CI (2012). Distributed synergistic plasticity and cerebellar learning. *Nat Rev Neurosci* **13**, 619–635.
- Gibson AR, Horn KM & Pong M (2004). Activation of climbing fibers. *Cerebellum* **3**, 212–221.
- Groenewegen HJ, Voogd J & Freedman SL (1979). The parasagittal zonation within the olivocerebellar projection. II. Climbing fiber distribution in the intermediate and hemispheric parts of cat cerebellum. *J Comp Neurol* **183**, 551–601.
- Halverson HE, Khilkevich A & Mauk MD (2015). Relating cerebellar Purkinje cell activity to the timing and amplitude of conditioned eyelid responses. *J Neurosci* **35**, 7813–7832.
- Harvey RJ & Napper RMA (1991). Quantitative studies on the mammalian cerebellum. *Prog Neurobiol* **36**, 437–463.
- Heffley W, Song EY, Xu Z, Taylor BN, Hughes MA, McKinney A, Joshua M & Hull C (2018). Coordinated cerebellar climbing fiber activity signals learned sensorimotor predictions. *Nat Neurosci* **21**, 1431–1441.
- Herzfeld DJ, Kojima Y, Soetedjo R & Shadmehr R (2018). Encoding of error and learning to correct that error by the Purkinje cells of the cerebellum. *Nat Neurosci* **21**, 736–743.
- Hilgard ER & Marquis DG (1936). Conditioned eyelid responses in monkeys, with a comparison of dog, monkey, and man. *Psychol Monogr* **47**, 186–198.
- Hoogland TM, De Gruijl JR, Witter L, Canto CB & De Zeeuw CI (2015). Role of synchronous activation of cerebellar Purkinje cell ensembles in multi-joint movement control. *Curr Biol* **25**, 1157–1165.
- Ito M (2003). Long-term depression. *Annu Rev Neurosci* **12**, 85–102.
- Ito M (2013). Error detection and representation in the olivo-cerebellar system. *Front Neural Circuits* **7**, 1.
- Ito M & Kano M (1982). Long-lasting depression of parallel fiber-Purkinje cell transmission induced by conjunctive stimulation of parallel fibers and climbing fibers in the cerebellar cortex. *Neurosci Lett* **33**, 253–258.
- Junker M, Endres D, Sun ZP, Dicke PW, Giese M & Thier P (2018). Learning from the past: a reverberation of past errors in the cerebellar climbing fiber signal. *PLoS Biol* **16**, e2004344.
- Kehoe EJ & Holt PE (1984). Transfer across CS-US intervals and sensory modalities in classical conditioning of the rabbit. *Animal Learning & Behavior* **12**, 122–128.
- Khosrovani S, Van Der Giessen RS, De Zeeuw CI & De Jeu MTG (2007). In vivo mouse inferior olive neurons exhibit heterogeneous subthreshold oscillations and spiking patterns. *Proc Natl Acad Sci U S A* **104**, 15911–15916.
- Kitazawa S, Kimura T & Yin PB (1998). Cerebellar complex spikes encode both destinations and errors in arm movements. *Nature* **392**, 494–497.
- Kubo R, Aiba A & Hashimoto K (2018). The anatomical pathway from the mesodiencephalic junction to the inferior olive relays perioral sensory signals to the cerebellum in the mouse. *J Physiol* **596**, 3775–3791.
- Lang EJ, Sugihara I, Welsh JP & Llinás R (1999). Patterns of spontaneous purkinje cell complex spike activity in the awake rat. *J Neurosci* **19**, 2728–2739.
- Leicht R, Rowe MJ & Schmidt RF (1973). Cortical and peripheral modification of cerebellar climbing fibre activity arising from cutaneous mechanoreceptors. *J Physiol* **228**, 619–635.
- Lim CCT & Lim SA (2009). Pendular nystagmus and palatomyoelonus from hypertrophic olivary degeneration. *New Engl J Med* **360**, e12.
- Llinás R & Volkind RA (1973). The olivo-cerebellar system: functional properties as revealed by harmaline-induced tremor. *Exp Brain Res* **18**, 69–87.
- Llinás R, Walton K, Hillman DE & Sotelo C (1975). Inferior olive: its role in motor learning. *Science* **190**, 1230–1231.
- Lock JT, Parker I & Smith IF (2015). A comparison of fluorescent Ca²⁺ indicators for imaging local Ca²⁺ signals in cultured cells. *Cell Calcium* **58**, 638–648.
- Mathy A, Clark BA & Häusser M (2014). Synaptically induced long-term modulation of electrical coupling in the inferior olive. *Neuron* **81**, 1290–1296.
- McCormick DA & Thompson RF (1984). Cerebellum: essential involvement in the classically conditioned eyelid response. *Science* **223**, 296–299.
- Miles TS & Wiesendanger M (1975). Organization of climbing fibre projections to the cerebellar cortex from trigeminal cutaneous afferents and from the SI face area of the cerebral cortex in the cat. *J Physiol* **245**, 409–424.
- Montarolo PG, Palestini M & Strata P (1982). The inhibitory effect of the olivocerebellar input on the cerebellar Purkinje cells in the rat. *J Physiol* **332**, 187–202.
- Mukamel EA, Nimmerjahn A & Schnitzer MJ (2009). Automated analysis of cellular signals from large-scale calcium imaging data. *Neuron* **63**, 747–760.
- Najafi F, Giovannucci A, Wang SSH & Medina JF (2014). Coding of stimulus strength via analog calcium signals in Purkinje cell dendrites of awake mice. *eLIFE* **3**, e03663.
- Negrello M, Warnaar P, Romano V, Owens CB, Lindeman S, Iavarona E, Spanke JK, Bosman LWJ & De Zeeuw CI (2019). Quasiperiodic rhythms of the inferior olive. *bioRxiv*, 408112.
- Ohmae S & Medina JF (2015). Climbing fibers encode a temporal-difference prediction error during cerebellar learning in mice. *Nat Neurosci* **18**, 1798–1803.
- Oscarsson O (1969). Termination and functional organization of the dorsal spino-olivocerebellar path. *J Physiol* **200**, 129–149.
- Ozden I, Dombeck DA, Hoogland TM, Tank DW & Wang SS (2012). Widespread state-dependent shifts in cerebellar activity in locomoting mice. *PLoS One* **7**, e42650.

- Ozden I, Lee HM, Sullivan MR & Wang SSH (2008). Identification and clustering of event patterns from in vivo multiphoton optical recordings of neuronal ensembles. *J Neurophysiol* **100**, 495–503.
- Ozden I, Sullivan MR, Lee HM & Wang SSH (2009). Reliable coding emerges from coactivation of climbing fibers in microbands of cerebellar Purkinje neurons. *J Neurosci* **29**, 10463–10473.
- Person AL & Raman IM (2011). Purkinje neuron synchrony elicits time-locked spiking in the cerebellar nuclei. *Nature* **481**, 502–505.
- Rahmati N, Owens CB, Bosman LWJ, Spanke JK, Lindeman S, Gong W, Potters JW, Romano V, Voges K, Moscato L, Koekkoek SKE, Negrello M & De Zeeuw CI (2014). Cerebellar potentiation and learning a whisker-based object localization task with a time response window. *J Neurosci* **34**, 1949–1962.
- Romano V, De Propriis L, Bosman LWJ, Warnaar P, ten Brinke MM, Lindeman S, Ju C, Velauthapillai A, Spanke JK, Middendorp Guerra E, Hoogland TM, Negrello M, D'Angelo E & De Zeeuw CI (2018). Potentiation of cerebellar Purkinje cells facilitates whisker reflex adaptation through increased simple spike activity. *eLife* **7**, e38852.
- Roome CJ & Kuhn B (2018). Simultaneous dendritic voltage and calcium imaging and somatic recording from Purkinje neurons in awake mice. *Nat Commun* **9**, 3388.
- Ruigrok TJH (2011). Ins and outs of cerebellar modules. *Cerebellum* **10**, 464–474.
- Ruigrok TJH, de Zeeuw CI, van der Burg J & Voogd J (1990). Intracellular labeling of neurons in the medial accessory olive of the cat: I. Physiology and light microscopy. *J Comp Neurol* **300**, 462–477.
- Rushmer DS, Woollacott MH, Robertson IT & Laxer KD (1980). Somatotopic organization of climbing fiber projections from low threshold cutaneous afferents to pars intermedia of cerebellar cortex in the cat. *Brain Res* **181**, 17–30.
- Samuel M, Torun N, Tuite PJ, Sharpe JA & Lang AE (2004). Progressive ataxia and palatal tremor (PAPT): clinical and MRI assessment with review of palatal tremors. *Brain* **127**, 1252–1268.
- Sasaki K, Bower JM & Llinás R (1989). Multiple Purkinje cell recording in rodent cerebellar cortex. *Eur J Neurosci* **1**, 572–586.
- Schultz SR, Kitamura K, Post-Uiterweer A, Krupic J & Häusser M (2009). Spatial pattern coding of sensory information by climbing fiber-evoked calcium signals in networks of neighboring cerebellar Purkinje cells. *J Neurosci* **29**, 8005–8015.
- Shambes GM, Gibson JM & Welker W (1978). Fractured somatotopy in granule cell tactile areas of rat cerebellar hemispheres revealed by micromapping. *Brain Behav Evol* **15**, 94–140.
- Simpson JL, Wylie DR & De Zeeuw CI (1996). On climbing fiber signals and their consequence(s). *Behav Brain Sci* **19**, 384–398.
- Snider RS & Stowell A (1944). Receiving areas of the tactile, auditory and visual system in the cerebellum. *J Neurophysiol* **7**, 331–357.
- Stotolo C, Llinás R & Baker R (1974). Structural study of inferior olivary nucleus of the cat: morphological correlates of electrotonic coupling. *J Neurophysiol* **37**, 541–559.
- Stosiek C, Garaschuk O, Holthoff K & Konnerth A (2003). In vivo two-photon calcium imaging of neuronal networks. *Proc Natl Acad Sci U S A* **100**, 7319–7324.
- Streng ML, Popa LS & Ebner TJ (2017). Climbing fibers control Purkinje cell representations of behavior. *J Neurosci* **37**, 1997–2009.
- Sugihara I, Fujita H, Na J, Quy PN, Li BY & Ikeda D (2009). Projection of reconstructed single Purkinje cell axons in relation to the cortical and nuclear aldolase C compartments of the rat cerebellum. *J Comp Neurol* **512**, 282–304.
- Sugihara I, Marshall SP & Lang EJ (2007). Relationship of complex spike synchrony bands and climbing fiber projection determined by reference to aldolase C compartments in crus IIa of the rat cerebellar cortex. *J Comp Neurol* **501**, 13–29.
- Sugihara I, Wu H & Shinoda Y (1999). Morphology of single olivocerebellar axons labeled with biotinylated dextran amine in the rat. *J Comp Neurol* **414**, 131–148.
- Sugihara I, Wu HS & Shinoda Y (2001). The entire trajectories of single olivocerebellar axons in the cerebellar cortex and their contribution to cerebellar compartmentalization. *J Neurosci* **21**, 7715–7723.
- Sullivan MR, Nimmerjahn A, Sarkisov DV, Helmchen F & Wang SSH (2005). In vivo calcium imaging of circuit activity in cerebellar cortex. *J Neurophysiol* **94**, 1636–1644.
- Suvrathan A, Payne HL & Raymond JL (2016). Timing rules for synaptic plasticity matched to behavioral function. *Neuron* **92**, 959–967.
- Szentágothai J (1965). The use of degeneration methods in the investigation of short neuronal connexions. *Prog Brain Res* **14**, 1–32.
- Tada M, Takeuchi A, Hashizume M, Kitamura K & Kano M (2014). A highly sensitive fluorescent indicator dye for calcium imaging of neural activity in vitro and in vivo. *Eur J Neurosci* **39**, 1720–1728.
- Ten Brinke MM, Boele HJ & De Zeeuw CI (2019). Conditioned climbing fiber responses in cerebellar cortex and nuclei. *Neurosci Lett* **688**, 26–36.
- Ten Brinke MM, Boele HJ, Spanke JK, Potters JW, Kornysheva K, Wulff P, Ijpelaar ACHG, Koekkoek SKE & De Zeeuw CI (2015). Evolving models of Pavlovian conditioning: cerebellar cortical dynamics in awake behaving mice. *Cell Rep* **13**, 1977–1988.
- Thach WT Jr (1967). Somatosensory receptive fields of single units in cat cerebellar cortex. *J Neurophysiol* **30**, 675–696.
- Tsutsumi S, Yamazaki M, Miyazaki T, Watanabe M, Sakimura K, Kano M & Kitamura K (2015). Structure–function relationships between aldolase C/zebrin II expression and complex spike synchrony in the cerebellum. *J Neurosci* **35**, 843–852.
- Van Der Giessen RS, Koekkoek SK, van Dorp S, De Grijl JR, Cupido A, Khosrovani S, Dortland B, Wellershaus K, Degen J, Deuchars J, Fuchs EC, Monyer H, Willecke K, De Jeu MTG & De Zeeuw CI (2008). Role of olivary electrical coupling in cerebellar motor learning. *Neuron* **58**, 599–612.

- Voges K, Wu B, Post L, Schonewille M & De Zeeuw CI (2017). Mechanisms underlying vestibulo-cerebellar motor learning in mice depend on movement direction. *J Physiol* **595**, 5301–5326.
- Voogd J & Glickstein M (1998). The anatomy of the cerebellum. *Trends Neurosci* **21**, 370–375.
- Wang JJ, Kim JH & Ebner TJ (1987). Climbing fiber afferent modulation during a visually guided, multi-joint arm movement in the monkey. *Brain Res* **410**, 323–329.
- Welsh JP, Ahn ES & Placantonakis DG (2005). Is autism due to brain desynchronization? *Int J Dev Neurosci* **23**, 253–263.
- Welsh JP, Lang EJ, Sugihara I & Llinas R (1995). Dynamic organization of motor control within the olivocerebellar system. *Nature* **374**, 453–457.
- Witter L, Canto CB, Hoogland TM, de Gruijl JR & De Zeeuw CI (2013). Strength and timing of motor responses mediated by rebound firing in the cerebellar nuclei after Purkinje cell activation. *Front Neural Circuits* **7**, 133.
- Wylie DR, De Zeeuw CI & Simpson JJ (1995). Temporal relations of the complex spike activity of Purkinje cell pairs in the vestibulocerebellum of rabbits. *J Neurosci* **15**, 2875–2887.
- Xiao J, Cerminara NL, Kotsurovskyy Y, Aoki H, Burroughs A, Wise AK, Luo Y, Marshall SP, Sugihara I, Apps R & Lang EJ (2014). Systematic regional variations in Purkinje cell spiking patterns. *PLoS One* **9**, e105633.
- Yang Y & Lisberger SG (2014). Purkinje-cell plasticity and cerebellar motor learning are graded by complex-spike duration. *Nature* **510**, 529–532.
- Yatim N, Billig I, Compoin C, Buisseret P & Buisseret-Delmas C (1996). Trigemino-cerebellar and trigemino-olivary projections in rats. *Neurosci Res* **25**, 267–283.
- Zhou H, Lin Z, Voges K, Ju C, Gao Z, Bosman LWJ, Ruigrok TJH, Hoebeek FE, De Zeeuw CI & Schonewille M (2014). Cerebellar modules operate at different frequencies. *eLIFE* **3**, e02536.

Additional information

Competing interests

The authors declare that there are no competing interests.

Author contributions

All experiments were performed at the Department of Neuroscience of the Erasmus MC, Rotterdam, the Netherlands. The experiments were designed by C.J., L.W.J.B., T.M.H., P.M., M.N. and C.I.D.Z., performed by C.J. and P.M. and analysed by all authors. The manuscript was written by C.J., L.W.J.B., T.M.H., M.N. and C.I.D.Z. with contributions from all authors. All authors have approved the final version of the manuscript and ensure the accuracy and integrity of the data presented. All persons with a significant contribution to this study are listed as authors.

Funding

Financial support was provided by the Netherlands Organization for Scientific Research (NWO-ALW; C.I.D.Z.), the Dutch Organization for Medical Sciences (ZonMW; C.I.D.Z.), Life Sciences (C.I.D.Z.), ERC-adv and ERC-POC (C.I.D.Z.) and the China Scholarship Council (No. 2010623033; C.J.). The funders had no role in study design, data collection and analysis, decision to publish, or preparation of the manuscript.

Acknowledgements

We thank A.C.H.G. IJpelaar for technical assistance and Dr M. Schonewille for help with recording ocular movements during stimulation.